UNIVERSITY
OF OSLO

Mohammad Amin Razbani

Numerical Modelling of Mineral-Microbe Interactions

Investigation on microbially induced calcium carbonate precipitation

Thesis submitted for the degree of Philosophiae Doctor

Department of Physics
Faculty of Mathematics and Natural Sciences

2023

Series of dissertations submitted to the
Faculty of Mathematics and Natural Sciences, University of Oslo
No. 2724

ISSN 1501-7710

Cover: UiO.
Print production: Graphic center, University of Oslo.

To my beloved mom

Acknowledgements

Being a human entails going through lots of ups and downs in life, so did I through this PhD project. In this journey, you feel lucky when you encounter some virtuous souls who give you new dimensions you're likely to carry til the rest of your life. I hope that words I'm going to spell can show the depth of gratitude I have for all who stood with me in this quest.

First things first, this work was funded by the project BioZEment 2.0 (grant number 269084), distributed by the Research Council of Norway. As a PhD student I was honored to be a member of Njord center, formerly known as PGP. I cannot overstate how lively and friendly the PGP was for a fresh PhD student when I first started my job.

I offer my special thanks to my main supervisor Anja Røyne. Anja, I appreciate all your help and insights throughout this project. Your availability , open-mindedness, and constructive criticism were fundamental for me to reach this point. I extend my gratitude to Enspen Jettestuen, my co-supervisor, for his patience with all of my basic and sometime repetitive questions.

Coming from 37 degrees latitude all the way to 60 degrees was a huge change for me. I cannot imagine how I would have endured long, dark, and cold winters of the north without the open, bright, and warm hearts of my friends here in Oslo.

Last but certainly not least, I want to express my heartfelt gratitude to my mom, whose unconditional love has been the most precious gift throughout my life. Finally, I would like to honor the memory of my father, whose wisdom and inspiration continue to resonate within me.

Mohammad Amin Razbani
Oslo, December 2023

Contents

Chapter 1

Introduction

1.1 Motivation

Until recently, natural geological processes were the primary drivers of changes in the Earth's shape and atmosphere. Now, human activities are considered the main drivers, leading us to the age of the Anthropocene. One of the most significant threats of modern civilization is climate change, mainly caused by the excessive release of greenhouse gases from human activities, particularly industrial processes. Cement production is a major contributor to CO_2 emissions globally, accounting for 36% of emissions from construction activities in 2010 (Bajželj, Allwood, and Cullen 2013) and remains a significant source of emissions (International Energy Agency 2023).

Another aspect of the Anthropocene is soil erosion, which necessitates the stabilization of eroded land using soil improvement techniques to prevent further pollution. Society demands eco-friendly solutions to address these environmental challenges and mitigate the stress on natural systems, particularly in the fields of geotechnical engineering, construction industries, and soil improvement (Osinubi et al. 2020).

Biogenic calcium carbonate crystals are a common type of bio-minerals found in nature. This has inspired a lot of research to utilize microbially driven calcium carbonate crystallization for biocementation and bioremediation purposes (Eltarahony, Zaki, and Abd-El-Haleem 2020).

Biocementation is a process that uses microorganisms, often bacteria, to precipitate minerals, typically calcium carbonate, in soil or construction materials. This results in improved material strength and durability, making it valuable for applications like soil stabilization and construction. Bioremediation is an eco-friendly and sustainable method for cleaning up contaminated sites, using bacteria to transform or remove harmful substances, thus restoring the ecosystem.

Microbially induced calcium carbonate precipitation (MICP) is an eco-friendly technique that has gained popularity in recent years. Nemati 2003 first proposed this as a technique for modification of porosity and permeability of a porous media.

The most commonly used pathway for MICP is the ureolytic pathway. In this process, alkalophilic bacteria consume urea as a substrate in an enzymatic reaction involving the enzyme urease, resulting in an increase in pH. When there is sufficient calcium in the solution, calcium carbonate crystals precipitate. Precipitation of calcium carbonate, occurring within a porous bed of unconsolidated sand, binds the sand grains, forming biocement (Whiffin, Paassen, and Harkes 2007). Consequently, this process can significantly reduce the porosity and permeability of the medium.

MICP has been extensively studied and has shown promising results in various applications, including self-healing concrete (Wiktor and Jonkers 2011), fracture sealing (Cuthbert, McMillan, et al. 2013), soil improvement (Whiffin, Paassen, and Harkes 2007), and the remediation of heavy metals from water (Achal et al. 2012). Notable advantages of this method include its operation at room temperature without the need for additional energy input and utilization of inexpensive ingredients, such as urea and calcium-rich solutions, as well as naturally occurring bacteria (Gomez, Anderson, et al. 2017).

Another advantage that makes this method particularly suitable for soil improvement techniques is the slow rate of the cementation process and the low viscosity of the solution. These characteristics allow the solution to spread a significant distance from the injection point before solidification occurs (Paassen et al. 2010).

The challenges of the MICP technique primarily arise from the biotic aspects of the process. Maintaining the activity and efficiency of the bacteria during the ureolysis process can be challenging, as the bacteria can be lost over time due to encapsulation by calcite or their natural life cycle. Introducing fresh bacteria into the environment can increase the cost of the process. Another limitation is that the material's pore size must fall within a specific range (0.5-2 micrometers) for the bacteria to move freely (Ivanov and Chu 2008).

The mechanical strength of the final material is typically weaker compared to conventional concrete, with most studies reporting an unconfined compressive strength (UCS) ranging from 1-10 MPa for cemented samples (Almajed et al. 2019). In contrast, conventional concrete typically has a UCS of around 40 MPa. However, Mujah, Cheng, and Shahin 2019 demonstrated that, for soil stabilization applications, MICP can provide a UCS as high as 1.5 MPa at 6% $CaCO_3$, while ordinary Portland cement provides 650 kPa UCS at the same cement content. Some MICP products available in the market claim to achieve UCS values as high as 30 MPa (*Biolith® Tile from Biomason* 2022).

MICP is a complex process that involves both biotic and abiotic components, with reactions occurring at varying speeds. The process can be studied at various scales, from the micro to the macro, making it challenging to explain. Modeling techniques have been employed to elucidate how different processes interact. Addressing pore-scale processes is more challenging than addressing macro-scale processes.

Macro-scale models rely on certain estimations derived from a pore-scale understanding of the system, including the porosity-permeability relationship, bacterial distribution, nucleation pattern of calcite, and available reactive surfaces. However, the correlation between pore-scale and macro-scale parameters remains an area that necessitates additional research due to its relatively limited exploration. Direct numerical simulation (DNS) of MICP serves as the ultimate tool for developing a bottom-up understanding of the process.

Macro-scale modeling has been explored in numerous studies. However, many of these models pose challenges for other researchers to utilize and test. Additionally, they often lack a geochemical solver, instead relying on simplified chemistry.

In this project, our primary objective is to perform DNS of MICP at the pore-scale. To accomplish this, we will utilize an advanced geochemical solver to account for the complex chemistry involved. Our goal is to develop an integrated simulation tool that encompasses ureolysis, geometry evolution, biomass placement, and transport within the system. This tool will enable us to tackle some of the challenges associated with understanding MICP at the pore-scale.

Furthermore, we will create a macro-scale model for MICP using the standard geochemical solver, Phreeqc (Parkhurst and Appelo 2013). Our aim is to provide a straightforward yet accurate simulation tool for MICP at the Darcy-scale that can be readily used by researchers and enthusiasts in the field.

In Fig. 1.1, the multi-scale approach to MICP is schematically depicted. The plot on the left side of the column shows the macro-scale model's predictions for the average concentration of calcite at different locations within a test tube where MICP is performed. The image on the right side of the column displays predictions from the pore-scale simulator. Grey patches represent sand grains, red indicates calcite, and yellow squares depict biomass locations. The resolution of the pore-scale simulation is 100 μm, while the macro-scale is on the order of meters.

Finally, we will develop a biocementation simulator with optimization metrics to determine the most effective treatment strategy based on the desired outcome.

1.2 Structure of the thesis

In the next chapter, I will present background information on modeling MICP and related topics. Additionally, I will outline the research questions that I aim to address.

Chapter 3 will provide a detailed explanation of the lattice Boltzmann (LB) method, which is the numerical method utilized for pore-scale modeling. In Chapter 4, I will summarize my papers and manuscripts, and describe our approach to addressing and resolving the research questions that have been raised.

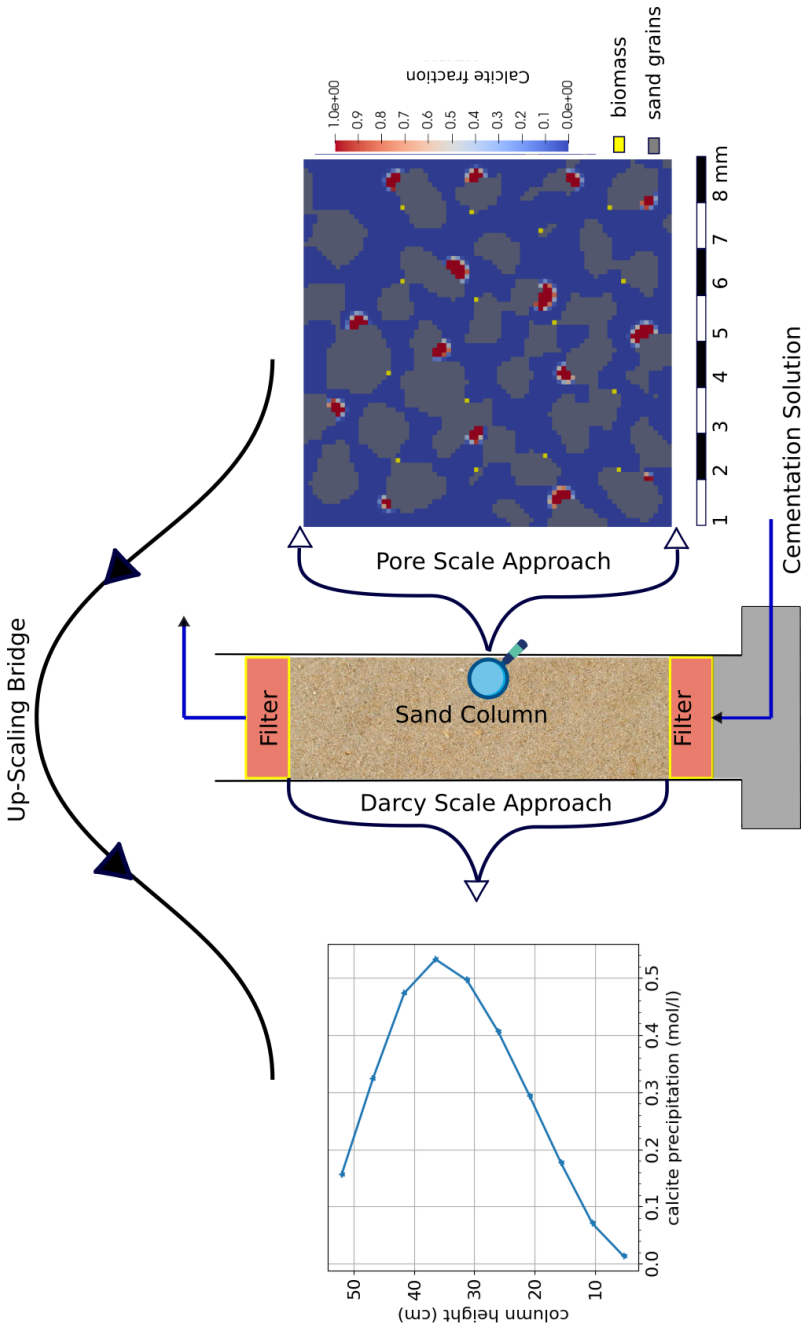

Figure 1.1: Multi-scale approach to MICP in this thesis. The graph comes from macro-scale modelling while the porous structure is represented using pore scale approach.

Chapter 2

Background

In this chapter, I will offer a more detailed explanation of MICP. I will examine both the geochemical and biological aspects of this process and outline its applications. Furthermore, I will review the literature on modeling MICP and identify the challenges and issues associated with the process.

2.1 Biocementation as a biogeochemical process

MICP consists of two main steps. The first step involves an increase in the inorganic carbon content of the medium in the form of carbonate, which in this work is achieved through the hydrolysis of urea (ureolysis). The second step involves the precipitation of calcium carbonate, which leads to a decrease in the porosity and permeability of the porous medium. In the context of cementation techniques, the overall process is referred to by different names in the literature, including biocement, biocementation, and biogrout. In this work, we use the terms "biocement" and "biocementation." The following two reactions describe MICP through ureolysis:

$$\mathrm{CO(NH_2)_2 + 2H_2O \xrightarrow{urease} CO_3^{-2}(aq) + 2NH_4^+(aq)}, \tag{2.1}$$

$$\mathrm{Ca^{2+}(aq) + CO_3^{2-}(aq) \leftrightarrow CaCO_3(s)}. \tag{2.2}$$

Urea ($\mathrm{CO(NH_2)_2}$) is hydrolyzed using the enzyme urease that is produced by the bacteria. Ureolysis is an irreversible reaction. On the other hand, the precipitation of calcium carbonate is a reversible reaction and its direction depends on the saturation ratio (SR) of calcium carbonate. The SR for calcium carbonate is defined as follows:

$$\gamma = \frac{a_{CO_3^{2-}} \cdot a_{Ca^{2+}}}{K}, \tag{2.3}$$

in which, γ is the SR, $a_{CO_3^{2-}}$ and $a_{Ca^{2+}}$ are the activities of $\mathrm{CO_3^{2-}}$ and $\mathrm{Ca^{2+}}$, respectively, and K is the equilibrium constant for this reaction. For γ larger than one, Eq. 2.2 shifts to the right. Ureolysis increases the concentration of carbonate, which can cause γ to rise above one. Precipitation halts when γ reaches one, indicating equilibrium for calcium carbonate precipitation or dissolution. Both reactions, as described in Eqs. 2.1 and 2.2, are treated kinetically using rate equations.

In this work, we incorporate a geochemical solver in our calculations to account for all reactions and complexes formed in conjunction with Eqs. 2.1 and 2.2 in an aqueous solution. For a comprehensive list of reactions, please refer to the table 1 in paper I.

2.2 Implementation of biocementation

The practical implementation of MICP for biocementation involves several key steps, beginning with the inoculation of the porous medium with bacteria capable of facilitating the ureolysis process. In this initial stage, the selection of robust and urease-producing bacterial strains is crucial to ensure the efficiency of the biocementation process. Bacterial inoculation is often achieved through methods such as direct injection into the porous medium or by introducing bacterial suspensions into the fluid flowing through the medium (K. Zhang et al. 2023).

Once the bacteria are introduced, the continuous flow or stop-flow regimes are employed to manage the MICP process (B. C. Martinez et al. 2012). In a continuous flow setup, a continuous supply of reactants, including urea and calcium ions, is provided to sustain ureolysis and calcium carbonate precipitation over an extended period.

Conversely, the stop-flow regime involves intermittently supplying reactants to the system, allowing for specific periods of reaction followed by rest intervals. This approach is often employed to control the spatial distribution of calcium carbonate precipitation within the porous medium. The stop-flow regime is advantageous in scenarios where precise control over the biocementation pattern or when localized treatment of specific areas within the medium is desired.

These practical considerations in the implementation of MICP underscore the significance of tailored strategies for bacterial inoculation and the careful selection of flow regimes to optimize the effectiveness of biocementation in diverse geological and engineering applications.

2.3 Modeling biocementation

Modeling biocementation has been investigated extensively in the research literature. Published models in this domain can be classified based on the following criteria:

- The length scale of interest: Darcy-scale or pore-scale.
- The scope of the model: hydrochemical, mechanical, and biological.
- Sophistication of different solvers used: chemical solver, transport solver, metabolic calculations.
- Modeling approach: statistical or deterministic.

In this thesis, I focus solely on deterministic works. The aim of this thesis is to develop mechanistic, not statistical, relationships between the main parameters involved in MICP. I have compiled a list of relevant papers found in the literature, which present theoretical models for MICP, in Table 2.1, along with their identified features. The first paper in Table 2.1 is part of this thesis.

2.3.1 Pore-scale modeling

In pore-scale modeling of MICP, numerous studies have been conducted to comprehend the micro-scale parameters that influence the ultimate macro-scale characteristics of the medium.

A common theme in pore-scale modeling is the trade-off between the level of detail included to explain one aspect of the process versus ignoring other aspects. For example, Murugan et al. 2022 provided a sophisticated model for predicting urease activity by utilizing a genome-scale metabolic model for the bacteria's metabolism. However, this model for ureolysis is not coupled to a reactive transport model to see how such a model plays out on a larger scale. In another example, Nishimura and Matsubara 2021, by focusing on one pore, can provide stress-strain calculations in their structure. Still, as a consequence of focusing on one pore, they cannot introduce heterogeneity of biomass, pore geometry, and chemistry in their model. Examples of such trade-offs or focusing on one aspect can be found in other works as well (Tang et al. 2019; T. Zhang and Klapper 2014).

Trade-offs in including different aspects of the process or avoiding making a comprehensive pore-scale model for biocementation at the pore-scale are due to theoretical and practical difficulties in coupling different processes in one model, uncertainties in the parametrization of different effects at the pore-scale, and the computational cost of running such simulations.

Qin, Hassanizadeh, and Ebigbo 2016 provide the first pore-scale hydrochemical model of biocementation for a large domain of porous media. This work is more comprehensive in terms of covering the main elements of MICP at the pore-scale. However, due to the nature of their modeling method, pore-network, they suggest that some of their assumptions need to be confirmed by direct simulations. Pore-network models act as a bridge between DNS and Darcy-scale modeling.

Pore-scale studies on MICP indicate that the micro-environment surrounding biomass could be important in the rate of reactions and geometry evolution (Murugan et al. 2022; T. Zhang and Klapper 2014). However, the kinetics of precipitation appear to be less influential, as the process is primarily constrained by ureolysis (Qin, Hassanizadeh, and Ebigbo 2016). In terms of mechanical properties, it has been observed that accounting for the heterogeneity of the porous structure leads to more accurate predictions (Tang et al. 2019).

To investigate the evolution of micro-environments and achieve a realistic representation of porous structure heterogeneity, we have developed a simulator coupled with an advanced geochemical solver. This simulator is presented as the first paper in this thesis (Razbani, Jettestuen, and Røyne 2023). Our aim was to provide a simulator that includes all the main elements considered in Darcy-scale models, such as reactive transport, ureolysis, and mineral precipitation kinetic rates. Additionally, we incorporated other features available at the pore-scale, such as biomass placement, nucleation site distribution, and a realistic representation of geometry. Incorporating all these elements enables the model to properly upscale pore-scale phenomena and test Darcy-scale assumptions.

Table 2.1: Review of deterministic modeling works in MICP in the literature.

paper	length scale	modeling scope	chemical solver	transport solver	metabolic details
Razbani, Jettestuen, and Røyne 2023	pore-scale	bio-chemo-hydraulic	advanced	2D	simple
D. Feng et al. 2022	Darcy-scale	bio-chemo-hydraulic	advanced	2D	simple
Mehrabi and Atefi-Monfared 2022	Darcy-scale	bio-chemo-hydro-mechanical	simple	2D	simple
Murugan et al. 2022	pore-scale	biological	advanced	batch	advanced
Tveit and Landa-Marbán 2022 & Landa-Marbán et al. 2021	Darcy-scale	bio-chemo-hydraulic	simple	2D	simple
Nishimura and Matsubara 2021	pore-scale	bio-chemo-hydro-mechanical	simple	3D	simple
X. Wang and Nackenhorst 2020	Darcy-scale	bio-chemo-hydraulic	simple	1D	simple
Minto, Lunn, and El Mountassir 2019	Darcy-scale	bio-chemo-hydraulic	simple	3D	simple
Tang et al. 2019	pore-scale	mechanical	-	-	-
Tan et al. 2017	Darcy-scale	hydraulic	-	-	-
K. Feng, Montoya, and Evans 2017	pore-scale	mechanical	-	-	-
Qin, Hassanizadeh, and Ebigbo 2016	pore-scale	bio-chemo-hydraulic	advanced	2D	simple

Table 2.1: Review of deterministic modeling works in MICP in the literature.

paper	length scale	modeling scope	chemical solver	transport solver	metabolic details
Wijngaarden, Paassen, et al. 2016a & Wijngaarden, Paassen, et al. 2016b & Wijngaarden, Vermolen, et al. 2013 & Wijngaarden, Vermolen, et al. 2011 & Wijngaarden, Vermolen, et al. 2010	Darcy-scale	bio-chemo-hydraulic	simple	1D	simple
Hommel, Lauchnor, et al. 2015 & Hommel, Cunningham, et al. 2013 & Ebigbo et al. 2012	Darcy-scale	bio-chemo-hydraulic	simple	1D	simple
T. Zhang and Klapper 2014	pore-scale	bio-chemo-hydraulic	advanced	2D	simple
B. Martinez, DeJong, and Ginn 2014	Darcy-scale	bio-chemo-hydraulic	advanced	1D	simple
Cuthbert, Riley, et al. 2012	Darcy-scale	bio-chemo-hydraulic	simple	Batch-system	simple
Fauriel and Laloui 2012	Darcy-scale	bio-chemo-hydro-mechanical	simple	1D	simple
Wu et al. 2011	Darcy-scale	bio-chemo-hydraulic	advanced	1D	simple
Barkouki et al. 2011	Darcy-scale	bio-chemo-hydraulic	advanced	1D	simple
Dupraz et al. 2009	Darcy-scale	biochemical	advanced	batch	simple

2.3.2 Darcy-scale modeling

Out of the 27 papers listed in Table 2.1, 22 of them focus on studying MICP at the Darcy-scale. Darcy-scale models are preferred due to their direct relevance to the macro-scale and the ease of validation with experimental observations. However, it is crucial to acknowledge that these models operate under certain simplifying assumptions, especially with respect to the homogenization of processes that primarily occur at the pore-scale. Examples of such processes include biotic interactions, crystal nucleation, and growth.

In adopting the Darcy-scale approach, a key concept is the representative elementary volume (REV) (Lichtner 1985). Beyond the REV, the medium is considered a continuum, simplifying the representation of complex pore-scale phenomena. This simplification, while facilitating computational efficiency and model tractability, introduces inherent limitations.

The limitations imposed by the REV give rise to spatio-temporal constraints on the model resolution. In other words, the model's ability to capture fine details in both space and time is restricted beyond the scale defined by the REV. This constraint is particularly relevant when dealing with intricate processes like biotic interactions and crystal formation, which often exhibit localized and temporally dynamic behavior.

Consequently, the decision to adopt a Darcy-scale model with REV-based simplifications involves a trade-off between computational feasibility and the fidelity of representing pore-scale complexities. Depending on the objectives of the model, this simplification may or may not impact the accuracy of predictions.

Numerous sophisticated Darcy-scale models have been published, as listed in Table 2.1. Different solvers are used depending on the spatial dimension of their models, which may be one-dimensional (1D), two-dimensional (2D), or three-dimensional (3D). Advection transport is usually a critical component of these models, most of which are classified as reactive transport models. These models are tasked with solving the following equation:

$$\frac{\partial C_i}{\partial t} + \nabla \cdot (C_i \vec{v}) = \nabla \cdot (D_i \nabla C_i) + Q_i, \tag{2.4}$$

in which C_i is concentration of species i, v is the advection velocity, D_i is the diffusion constant, and Q_i is a source term for reactions. Eq. 2.4 is coupled with chemistry of the reactive solution and the advection is subjected to porosity permeability change.

Reactions crucial to MICP occur over a wide spatio-temporal range. Ureolysis takes place within biomass colonies and progresses very slowly, while the speciation of chemical complexes occurs rapidly throughout the aqueous solution. The precipitation of calcite, on the other hand, is influenced by both ureolysis and the availability of aqueous calcium in the solution.

In this context, various questions may arise, such as whether crystallization is limited by mass transfer, which reactions can be considered to be in equilibrium, what constitutes the limiting step in the entire process. Answering these questions relate to making better assumptions for our models specially in Darcy-scale and helps us to optimize the process for different purposes.

Among all the different aspects of MICP, modeling the ureolysis rate is particularly challenging. This difficulty arises from the fact that, unlike inorganic chemical components, it is hard to determine the biomass density and its evolution in the medium due to the complex nature of living organisms.

The other aspect of biomass evolution is growth and decay. Modeling decay is more straight forward and it is done using a first order decay rate (Ebigbo et al. 2012; Fauriel and Laloui 2012; X. Wang and Nackenhorst 2020).

Estimation of biomass density is done commonly through indirect methods. For example, B. C. Martinez et al. 2012 estimated initial concentration of the urease by using a proprietary geochemical solver called TOUGHREACT and a calibration tool called UCODE from experimental pH data. The other challenge is to estimate how the initial biomass density changes over the course of process. The biomass density can change due to encapsulation in calcite, lack of vital nutrients, or other more complicated biotic reasons. Such changes can significantly affect rate of ureolysis.

Geochemical calculations are in the core of any MICP model. Some studies used a simplified version and some others used advanced calculations with full speciation of all chemical components. Some advanced models use Phreeqc as their geochemical solver (D. Feng et al. 2022; B. Martinez, DeJong, and Ginn 2014; Qin, Hassanizadeh, and Ebigbo 2016; Weathers 2011). Phreeqc is a free and open-source standard geochemical solver that can be coupled with other simulators. The coupling adds to the computational time each time the phreeqc is called (D. Feng et al. 2022). There are other papers that used a software package called TOUGHREACT which is a proprietary software (Barkouki et al. 2011; B. Martinez, DeJong, and Ginn 2014; Wu et al. 2011).

Modeling field-scale application of MICP introduces more uncertainties. The difficulty of parameterization of biotic processes, or finding porosity-permeability relationship has led some researchers to encourage developing simple models that are computationally more efficient and can facilitate the use of MICP (Hommel, Lauchnor, et al. 2015).

This is precisely where the last two papers presented in this thesis come into play. We aim to address this gap by developing a simulator that is both easy to use and computationally fast, operating at the Darcy-scale. Through the utilization of such a simulator, we will provide optimization metrics and tools. The optimization step is an aspect that previous modeling works in the literature have not adequately addressed.

2.4 Biophysics of MICP

2.4.1 Metabolism

Just like any other living organism, bacteria require a continuous supply of energy to sustain their cellular processes. Unlike more complex life forms, bacteria do not possess mitochondria or chloroplasts for energy production; instead, they rely on external sources. Substrate, in the form of organic or inorganic compounds, serves as their primary source of energy.

Ureolysis is a metabolic pathway used by specific bacteria to obtain energy. Urea is enzymatically broken down into ammonia nitrogen source for respiration and carbon dioxide by the enzyme urease. This process releases energy, which the bacteria harness for their metabolic needs. Additionally, ammonia as a nitrogen source can be used for respiration (K. Zhang et al. 2023).

2.4.2 Distribution

Bacteria do not distribute themselves evenly within the context of MICP; rather, they tend to cluster together in distinct groups. This clustering phenomenon plays a pivotal role in determining whether these bacterial aggregates will ultimately evolve into biofilms or not (Lappin-Scott and Bass 2001).

The non-uniform dispersion of bacteria in MICP is a consequence of their intrinsic biological behavior and interaction patterns. Bacteria often exhibit chemotaxis (Dillon, Fauci, and Gaver 1995), a process where they move towards or away from specific chemical signals or other bacteria. This behavior can lead to the formation of localized bacterial clusters within an MICP environment.

These bacterial aggregates, while seemingly haphazard, can significantly impact the outcome of MICP processes. Depending on various factors such as the composition of the microbial community, the surrounding environmental conditions, and the availability of nutrients, these bacterial clusters may evolve into biofilms (Cuthbert, Riley, et al. 2012; Decho 2010).

Biofilms are intricate and highly structured communities of microorganisms, encased within a self-produced extracellular matrix. When bacterial aggregates transition into biofilms, they become embedded in this matrix, forming a cohesive and protective microbial community.

Ureolytic bacteria, through their metabolic activity, can create microenvironments within biofilms that are conducive to ureolysis and subsequent calcium carbonate precipitation. This localized activity enhances the stability and resilience of biofilms (Dong et al. 2022). Biofilm formation during MICP has the potential to reduce permeability, but the long-term durability of this effect remains uncertain (K. Zhang et al. 2023).

Bacteria can also exist in the form of microcolonies, which are clonal groups of cells limited in size, typically ranging from 100 to 200μm (Jeanson et al. 2015). In this form, unlike biofilms, microcolonies do not feature an extracellular matrix.

The dominance of either biofilm-driven or microcolony-based MICP, characterized by lower bacterial density and the absence of dense biofilm structures, depends on the environmental conditions. Key considerations include nutrient availability, temperature, physical disruptions, pH levels, and oxygen concentrations within the given context (Decho 2010).

Some studies have reported or modelled microcolony-based MICP without the presense of biofilm formation (Liu et al. 2023; Mehrabi and Atefi-Monfared 2022; Nishimura and Matsubara 2021). Conversely, in other studies, biofilms have been observed or incorporated into their experiments and models (Hommel,

Lauchnor, et al. 2015; Landa-Marbán et al. 2021; Tveit and Landa-Marbán 2022).

2.4.3 Transport

The transport of bacteria in porous media during MICP is influenced by the biological characteristics and activities of the bacteria themselves, leading to non-uniform distribution and complex interactions, in contrast to the transport of a conservative tracer which is passive, predictable, and uniform.

Bacterial cells can attach to the surfaces of porous media particles, which can significantly slow down their transport. Attachment is influenced by factors like surface properties, bacterial adhesion mechanisms, and the presence of extracellular polymeric substances (Torkzaban et al. 2008). Bacteria can also detach from surfaces under certain conditions, contributing to their mobility (Park, Lee, and Kim 2008).

Bacteria can grow and reproduce within porous media, leading to an increase in their population density over time. This growth can further impact their transport behavior and distribution in the subsurface (Tufenkji 2007).

Several papers have proposed models for biomass fixation on the porous medium in MICP. Typically, these models assume a first-order kinetic reaction for the attachment/detachment of bacteria on solid surfaces, which is a common approach in various studies (Ebigbo et al. 2012; Fauriel and Laloui 2012; X. Wang and Nackenhorst 2020). In these studies, attachment and detachment factors are introduced and calibrated using experimental data. In certain studies, the rate of attachment and detachment from the biofilm during MICP has been considered (Ebigbo et al. 2012; Qin, Hassanizadeh, and Ebigbo 2016).

Attachment primarily comes into play during the inoculation phase when biomass is introduced into the porous medium. Conversely, detachment tends to be more prominent during subsequent injection steps, such as during precipitation, primarily driven by the influence of water shear forces.

2.5 Mechanics and precipitation

The cumulative volume of calcium carbonate formed through the biocementation process fundamentally shapes the strength and overall structural characteristics of the treated medium. However, it is not the only factor. Different applications may necessitate tailored approaches to optimize the quantity, distribution, and size of the precipitated calcium carbonate, aligning the mechanical properties of the treated medium with the specific requirements of the intended use.

Various parameters are employed to measure and quantify the mechanical strength resulting from MICP. One of the primary parameters is compressive strength, which assesses the material's ability to withstand applied compressive loads. It is a crucial indicator, especially for applications involving soil stabilization or cementation. There is a direct correlation between calcium carbonate content of a cured specimen and its compressive strength (Whiffin, Paassen, and Harkes 2007).

In applications where MICP is used to strengthen porous materials, such as soils or concrete, a uniform distribution of calcium carbonate is often desirable. A consistent distribution helps provide even reinforcement, enhancing overall mechanical strength.

In contrast, in scenarios where MICP is employed for sealing purposes, such as in geotechnical applications, localized precipitation may be more advantageous. Here, the formation of calcium carbonate deposits in targeted areas can effectively block pore spaces and reduce permeability (Liu et al. 2023).

Apart from the distribution of calcium carbonate their size is important in the context of application and mechanics. The formation of calcium carbonate crystals is influenced by various factors, including temperature, urease activity, the presence of nucleation sites, pH levels, the extent of saturation, and the concentration of the cementation solution (Mujah, Shahin, and Cheng 2017). Typically, calcium carbonate crystals induced during MICP have dimensions ranging from a few micrometers to tens of micrometers, and there is potential for these crystals to aggregate (Perri et al. 2018).

In the pore-scale, fluctuations in cementation concentration and the specific structure of the nearby pores are important in the initiation of crystal formation, with areas characterized by lower fluid velocities tending to facilitate more frequent crystal nucleation (Liu et al. 2023).

For example, for geological CO_2 sequestration or optimal seal performance during MICP, it is advisable to ensure the deposition of smaller crystals in the vicinity of the wellbore area. Conversely, when addressing potential gas leakage pathways in faults and fractures, the formation of larger crystals is more conducive to achieving improved sealing results (Liu et al. 2023). Another study on MICP treatment of sandy soils revealed that with shorter injection intervals, the produced crystals were more numerous but smaller in size (Y. Wang et al. 2022). Their microscale experiments illustrated that the growth of larger crystals occurred at the expense of the dissolution of smaller crystals, irrespective of the concentration of the cementation solution. Additionally, they showed that larger crystals were associated with higher soil strength.

The calcite distribution may or may not depend on the distribution of biomass, depending on the treatment strategy. Qin, Hassanizadeh, and Ebigbo 2016 reported that in their model, the precipitation pattern was not sensitive to the distribution of biofilm during a stop-flow injection treatment. On the other hand, they reported that during a continuous injection strategy, calcite distribution was determined by the biofilm distribution.

Particle size and morphology of sand grains are additional factors in this context. Song et al. 2022 conducted a study comparing UCS after biocementation using spherical, semi-spherical, and angular aggregates. In the range of their study, they reported that for spherical and semi-spherical sand grains, UCS peaks at a certain size and subsequently declines with increasing size. In contrast, for angular aggregates, smaller particles lead to higher UCS. The study reveals distinct bonding mechanisms between sand particles based on morphology, explaining their results. Point bonding is the primary mechanism in spherical sands, creating discrete points of contact between particles. Conversely, planar

contact bonds indicate a larger effective cementation area between angular sand particles, leading to a higher UCS at lower precipitated calcite content comparing to point bonding.

Different effects and parameters discussed regarding precipitation patterns or crystal sizes have significant implications for the mechanical strength and applications of MICP, all of which have been studied in numerous publications (Almajed et al. 2019; Cui et al. 2017; Dadda et al. 2017; X. Zhang et al. 2020).

2.6 MICP field applications

A considerable amount of research and implementation efforts have been dedicated to exploring the application of MICP in diverse environments (Landa-Marbán et al. 2021; Minto, Lunn, and El Mountassir 2019; Nassar et al. 2018; J. Zhang, Su, and Li 2022). Field applications refer to the practical implementation of MICP techniques in real-world environments beyond laboratory settings.

A few examples of large-scale applications of MICP for biocementation are reported in the literature. The first large-scale industrial biocementation was performed by Van Paassen 2011. They successfully treated a 1000 m^3 volume at depths ranging from 3 to 20 m below the surface. Gomez, B. C. Martinez, et al. 2015 used biocementation for dust suppression on soil in test fields measuring 2.4 m $\times$ 4.9 m. They demonstrated that a 2.5 cm thickness of cementation can exhibit increased resistance to erosion for up to 298 days. Ghasemi and Montoya 2022 reported even more promising results using MICP for dust suppression and soil stabilization on a large scale. They observed a significant improvement in erodibility even after major storm events over the course of 331 days. In another example, Gomez, Anderson, et al. 2017 treated tanks with a diameter of 1.7 m and a depth of 0.3 m to compare the outcomes of a normal bacteria injection approach with a biostimulation approach, where native ureolytic microorganisms are stimulated to accomplish ureolysis.

One of the primary challenges of MICP field applications is the variability in bacterial activity, porosity, and environmental conditions, such as pH, temperature, and nutrient availability. These factors can significantly influence the efficiency and effectiveness of the biomineralization process (K. Zhang et al. 2023). Moreover, the selection and optimization of suitable bacteria strains and their concentrations are crucial for achieving desired outcomes. Additionally, scaling up the MICP technique from laboratory-scale experiments to field applications poses logistical and engineering challenges that require careful consideration (Miftah, Khodadadi Tirkolaei, and Bilsel 2020).

To successfully implement MICP in the field, several important factors need to be considered. First, a thorough understanding of the site-specific soil conditions and engineering requirements is essential to tailor the MICP process accordingly (Osinubi et al. 2020). Moreover, a systematic approach for the selection of appropriate bacteria strains, nutrient solutions, and injection techniques is vital for achieving optimal results. Conducting field trials will be costly and require substantial time investment. To study the effects of these parameters, developing

simulation tools to devise the optimal treatment strategy is a common practice (Landa-Marbán et al. 2021; Minto, Lunn, and El Mountassir 2019; Tveit and Landa-Marbán 2022).

The field-scale injection strategies for calcium carbonate precipitation through multiple wells demonstrate challenges in achieving consistent treatment across regions between wells. Minto, Lunn, and El Mountassir 2019 conducted field-scale simulations of a 18×18 m MICP for soil stabilization. they report that simultaneous injection presents efficiency but struggles with creating static areas with no flow. Sequential injection via one well at a time offers more uniform treatment but elongates the overall process. Balancing efficiency and uniformity in treatment remains a key consideration for effective MICP strategies.

The cementation solution can be administered through pressure-controlled and flow rate-controlled injection strategies, both have their own merits. Pressure-controlled injection is advantageous when treating near-surface zones to mitigate the risk of ground heave, as it ensures the starting pressure is never exceeded. It also enables the delivery of more reagents to areas with high initial porosity around the well, potentially leading to a more even final strength across the site. However, it involves varying injection volumes for each well and changing treatment volumes per cycle, which could increase the complexity of on-site reagent handling and preparation (Minto, Lunn, and El Mountassir 2019).

Biocementation and other MICP related techniques, despite being in the early stages of integration into industrial engineering applications, have already persuaded some researchers that they will become mainstream engineering technologies for the future (K. Zhang et al. 2023).

2.7 Aim and objectives

In this thesis, I aim to address the following key points:

1. Establishing a pore-scale simulator to demonstrate the role of pore-scale effects in MICP.

2. Investigating how the geochemical evolution of the system at the pore-scale differs from the Darcy-scale explanation. For example, we will explore the local chemistry surrounding biomass during the MICP process at the pore-scale.

3. Developing user-friendly Darcy-scale simulators to provide MICP researchers with free and open-source tools.

4. Identifying the essential metrics for optimizing MICP and developing tools to facilitate this optimization.

Chapter 3

Modeling tools

Simulation of MICP in pore-scale was performed using BADChIMP Simulator (Jettestuen 2022). This simulator is an open-source software that is based on LB method. It also includes a native advanced geochemical solver. The core components of this simulator, including reactive transport using LB method for mineral dissolution and precipitation, have been previously used and tested in different publications (Hiorth, Jettestuen, L. Cathles, et al. 2013; Hiorth, Jettestuen, L. M. Cathles, et al. 2010; Pedersen et al. 2014). In this work, a biomass model is built into the code to account for ureolysis and biomass distribution.

3.1 Lattice Boltzmann method

LB method is a bridge between kinetic theory of gases and hydrodynamics. We use the LB method to solve the diffusion equation:

$$\frac{\partial C_i}{\partial t} = \nabla \cdot (D_i \nabla C_i) + Q_i, \tag{3.1}$$

in which, C_i is the concentration of species i, t is time, and Q is the macro-scale source term. In the core of kinetics of gases lies the Boltzmann equation that is derived from first principles. Boltzmann equation explains the evolution of perfect gases in kinetic theory. In this equation, the evolution of a perfect gas is described by a distribution function (Golse 2005):

$$g = g(t, \mathbf{x}, \mathbf{v}) \tag{3.2}$$

in which, g is the density of gas particles at time t and location $\mathbf{x}$ that have the velocity of $\mathbf{v}$. By taking a total derivative of the distribution function, LB equation is derived:

$$\frac{\partial g}{\partial t} + v\frac{\partial g}{\partial x} + \frac{F}{\rho}\frac{\partial g}{\partial v} = \Omega, \tag{3.3}$$

in which, F is the body force, ρ is mass density, and Ω is the collision operator. Solving the Boltzmann equation analytically is very difficult. Instead, a numerical solution is relatively straight forward. In this numerical approach, the distribution function (denoted as g) is fully discretized. This means that time, location, and velocity are no more continuous.

In this work, the 2-dimensional formulation of LB will be explored. In this scheme, space is discretized into a grid composed of square cells, referred to as a lattice. In any cell, the mass density of species i is calculated as follows:

$$\rho_i = \sum_\alpha g_\alpha^i(\mathbf{x}, t). \tag{3.4}$$

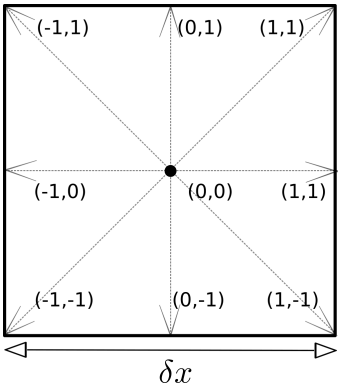

Figure 3.1: Basis velocity ($\mathbf{e}$) in nine directions in a node in LB method

In this approach, the discrete LB equation is defined as follows:

$$g_\alpha^i(\mathbf{x} + \mathbf{e}_\alpha \delta t, t + \delta t) - g_\alpha^i(\mathbf{x}, t) = \Omega_\alpha^i, \tag{3.5}$$

in which, $\mathbf{x}$ is the location of each node, and $\mathbf{e}$ is a basis velocity. α and i denote velocity direction and species, respectively. A node in LB method is represented in the Fig. 3.1. In this figure, arrows show the direction of α.

Eq. 3.5 describes the movement of particle distribution in the α direction to a new location after a time step δt with the velocity vector $\mathbf{e}_\alpha$. It also accounts for the adjustment of this distribution due to the collision operator Ω_i.

In our LB model, we restrict ourselves to a 2D non-advective system with nine velocity directions, as illustrated in Fig. 3.1. This setup is commonly referred to as D2Q9. The velocity directions as represented in Fig. 3.1 for this configuration are as follows:

$$\mathbf{e}_\alpha \in \{(0,0), (0,1), (1,0), (-1,0), (0,-1), (1,1), (1,-1), (-1,1), (-1,-1)\}. \tag{3.6}$$

The common choice of collision operator for Navier-Stokes simulations is the Bhatnagar-Gross-Krook (BGK) operator:

$$\Omega_\alpha^i = -\frac{\delta t}{\tau}[g_\alpha^i(\mathbf{x}, t) - g_\alpha^{i,eq}(\rho)] + \Delta\Omega_\alpha^i, \tag{3.7}$$

in which, τ is the relaxation time, and $\Delta\Omega$ is the source term. BGK operator relaxes the distribution towards an equilibrium distribution. The equilibrium distribution is calculated as follows:

$$g_i^{eq} = w_\alpha C_i, \tag{3.8}$$

$$w_\alpha \in [\frac{4}{9}, \frac{1}{9}, \frac{1}{9}, \frac{1}{9}, \frac{1}{9}, \frac{1}{36}, \frac{1}{36}, \frac{1}{36}, \frac{1}{36}], \tag{3.9}$$

in which w is called the wight of a lattice. Lattice source term is calculated from the macro source term as follows:

$$\Delta\Omega_\alpha^i = w_\alpha \left(1 + \frac{1}{2\tau}\right) Q_i \delta t. \tag{3.10}$$

Concentration and diffusion coefficient in macro-scale is calculated by

$$C_i = \sum_\alpha g_\alpha^i + \frac{1}{2} Q_i \delta t, \tag{3.11}$$

$$D = \frac{1}{3}(\tau - \frac{1}{2})\frac{\delta x^2}{\delta t}. \tag{3.12}$$

In the case of MICP, for urea, the source term Q is coupled to the concentration of urea (C). Therefore Eq. 3.11 cannot be solved to obtain C. We need to use the equation of the kinetics of ureolysis that connects Q to C in this case. Then we get two equations with two unknowns that can be solved for finding C and Q. The full derivation is presented in the paper I section 2.4.

3.1.1 Collision and Propagation

LB method is commonly described as a two step process, namely collision and propagation. In this way, the Eq. 3.5 is performed in two steps.

The collision step is where we account for the interactions between particles in our system. In the LB method, we use a collision operator (Equation 3.7) to adjust the distribution of particles at each lattice node. The relaxation time (τ) controls how quickly the distribution approaches an equilibrium state. The equilibrium distribution (Equation 3.8) is determined by the concentration of species (C_i) and weights (w_α) associated with each velocity direction. The collision operator gradually relaxes the particle distribution toward this equilibrium distribution. The distributions after collision are calculated based on Eq. 3.5 as follows:

$$g_\alpha^{i,*}(\mathbf{x}, t) = g_\alpha^i(\mathbf{x}, t) + \Omega_\alpha^i, \tag{3.13}$$

where $g_\alpha^{i,*}(\mathbf{x}, t)$ is collision distribution.

After the collision step, we move to the propagation step. In this step, we update the distribution of particles at each lattice node based on their current state. Each particle is propagated in a specific direction (denoted by α) with a characteristic velocity ($\mathbf{e}_\alpha$) over a small time interval (δt). Again, according to Eq. 3.5, propagation is performed based on the following equation:

$$g_\alpha^i(\mathbf{x} + \mathbf{e}_\alpha \delta t, t + \delta t) = g_\alpha^{i,*}(\mathbf{x}, t). \tag{3.14}$$

By repeating the collision and propagation steps over many time steps, we can simulate the behavior of particles in a lattice grid, which represents the diffusion process in our system. The LB method's numerical approach offers an efficient way to model complex systems, making it a valuable tool in various scientific and engineering applications.

For a more comprehensive understanding of the LB method and its equations, you can refer to the full derivation in Aursjø et al. 2017.

3.1.2 Boundary conditions

At the fluid-mineral interface, it's essential to apply an appropriate boundary condition. This boundary condition determines the flux that leaves the surface. When there is no reaction at the interface, the 'bounce-back' boundary condition is applied. In this case, the flux leaving the surface is equal to the flux that hit the surface one time step earlier. However, when the distribution of a species is reacting with the surface, a boundary condition that accounts for the kinetics of that reaction should be utilized.

There are different approaches for treating heterogeneous reactions in LB method. A link-based method is used in this paper. In this method, the outgoing flux in a specific direction from a wall node is calculated based on the incoming flux from the neighboring node at the opposite direction (Verhaeghe et al. 2006). You can see schematic representation of a wall node and fluxes perpendicular to the interface in Fig. 3.2. In this figure, $g^i_\alpha(x,t)$ is the known concentration distribution that departs the node and streams into to a virtual node inside the wall after one time step. This virtual flux is denoted as $\tilde{g}^i_\alpha(x+\delta x, t+\delta t)$. The difference between $g^i_{\bar{\alpha}}(x,t+\delta t)$, which is the concentration flux leaving the surface, and $\tilde{g}^i_\alpha(x+\delta x, t+\delta t)$ should be equal to the amount of dissolution or precipitation (Verhaeghe et al. 2006):

$$g^i_{\bar{\alpha}} - \tilde{g}^i_\alpha = 6 w_\alpha \mathbf{e}_\alpha R_i \mathbf{n}, \tag{3.15}$$

$$R_i = R_i(c_1, c_2, c_3, ..., c_n), \tag{3.16}$$

in which $\mathbf{n}$ in the the normal vector on the interface. R_i is reaction rate which is a function of the concentration of n different species at the interface. To find the concentration, we need the following equation that is derived from Eq. 3.5-3.8 (Verhaeghe et al. 2006):

$$g^i_{\bar{\alpha}} + \tilde{g}^i_\alpha = 2 w_\alpha c_i(t+\delta t, x+\delta x). \tag{3.17}$$

By using a reaction rate equation for R, $g^i_\alpha(x,t)$ and $c_i(t+\delta t, x+\delta x)$ can be calculated. The rate equations found in literature should be converted to LB units before it is used in Eq.3.15, because space and time are discretized in LB method. Therefore, real units for time and length in rate equation should be divided by δt, and δx with the same unit, respectively.

3.1.3 The pore-scale MICP Simulator

This section explains how the pore-scale simulator performs calculations and updates concentrations of different species.

In the first step, initial conditions are read from an input file. This file includes the concentration of bulk chemistry, kinetic constants for ureolysis and precipitation, and physical parameters like the diffusion coefficient. The chemical components considered in our work are carbon, calcium, ammonium, chloride, and urea. The complete set of reactions involving these species is presented in the paper I. Two geometry files are fed into the simulation—one showing the

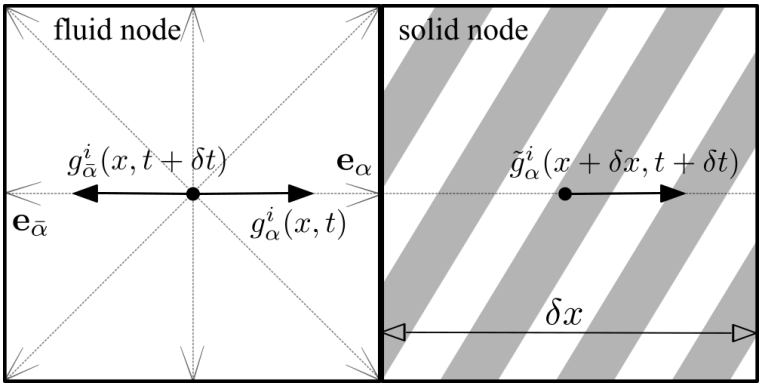

Figure 3.2: Evolution of distribution function at the solid-fluid interface for moving boundaries.

location of sand grains plus nucleation sites, and the other showing the location of biomass. The spatial resolution is another input in the geometry files.

After reading the input files, the distribution function is initialized by converting macro-scale input parameters into their lattice counterparts. This is done using Eq. 3.8. In another step, the time step (δt) is calculated using Eq. 3.12.

Then, Q in Eq. 3.11 for ureolysis is calculated in the biomass solver, as presented in the paper I section 2.4.

With the distribution function and source terms in hand, the collision step is performed based on Eq. 3.7. Afterward, the distribution is propagated into neighboring nodes. It is at this step that boundary conditions need to be taken into account, as presented in Fig. 3.2, where $g^i_{\bar{\alpha}}(x, t+\delta t)$ is unknown during the propagation step. Using the boundary condition presented in Eq. 3.15, the value of $g^i_{\bar{\alpha}}(x, t+\delta t)$ can be calculated.

To calculate $g^i_{\bar{\alpha}}(x, t+\delta t)$ based on Eq. 3.15, we need to know R, which is the rate of reaction. The reaction here is the precipitation of calcite. It is at this step that the geochemical solver comes into play. The geochemical solver takes the concentration of species from the LB solver and first calculates the concentration of complexes and saturation index of minerals—in this case, calcite.

Geometry evolution occurs when a bulk node is filled with calcite more than 50%. In this case, a bulk node is turned into a solid node.

With all distributions found, the propagation step is accomplished, marking the end of one time step in the simulation. At this step, the termination criterion is checked, and if it is not met, time is increased by δt, and another round of collision propagation will be performed.

3.2 Native geochemical solver

The geochemical calculations are handled by a native chemical solver (Hiorth, Jettestuen, L. Cathles, et al. 2013) embedded in the BADChIMP simulator (Jettestuen 2022). The geochemical solver rely on a database of some basis species which refer to a set of chemically simple and well-defined chemical species that serve as a foundation or reference point for describing the behavior of more complex chemical species or complexes in a solution. These basis species are chosen because their thermodynamic properties, such as standard Gibbs free energy of formation and dissociation constants, are well-documented and readily available.

More complex chemical species or complexes in the system can be represented in terms of their relationships to the basis species. This is typically done by specifying how they are formed or dissociate into combinations of the basis species.

Given the concentrations of the basis species and the relevant dissociation constants (log Ks), the concentrations of the secondary species or complexes can be calculated using principles of chemical equilibrium and thermodynamics. This is done using the mass action law. For more information, refer to Lichtner, Steefel, and Oelkers 2019 where a complete formulation of multi-component reactive transport is presented.

There are homogeneous reactions that happen in the bulk of the fluid and heterogeneous reactions that happen at the interface of fluid and solid in our work. The homogeneous reactions are assumed to be in instantaneous equilibrium and mineral precipitation as a heterogeneous reaction is kinetically controlled.

The geochemical solver comes into play when we want to solve Eq. 3.15, 3.16, and 3.17.

3.3 Benchmarking LB transport solver

The LB transport solver was benchmarked against an analytical solution for reaction diffusion from a semi-finite surface. In this case, a first order surface reaction happens on a semi-finite surface and a chemical compound is released and diffuses into the bulk. To find the concentration of the released component in time and space, the following equation should be solved:

$$\frac{\partial C}{\partial t} = D\frac{\partial^2 C}{\partial x^2}, \tag{3.18}$$

$$C = C_0 \quad \text{when} \quad t = 0,$$

$$D\frac{\partial C}{\partial x} = k(C - C_{eq}) \quad \text{when} \quad x = 0.$$

C_0 represents the initial concentration, set to 1e-8 in our simulation. The rate constant, denoted as k, is 0.1 s^{-1}, and C_{eq} stands for the equilibrium concentration, which is 0.1 M. The analytical solution for Eq. 3.18 with its

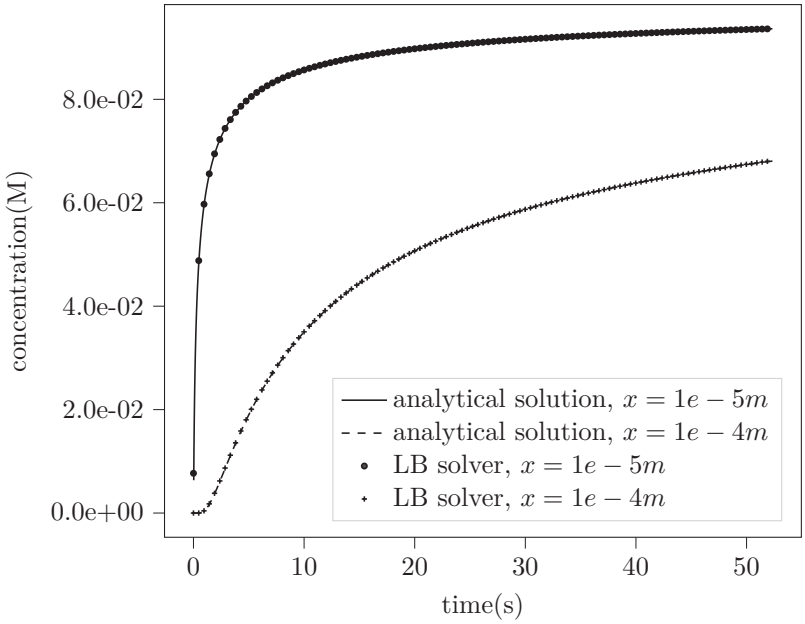

Figure 3.3: Comparing analytical solution versus numerical solution from LB solver

corresponding initial conditions was obtained from the literature (Carslaw and Jaeger 2011).

In Fig. 3.3, a comparison between the analytical solution and the result from the LB solver is presented at two different distances from the surface. It is evident that the LB transport solver can effectively solve Eq. 3.18.

3.4 Phreeqc software

Phreeqc is an open-source computer program that is widely used for modeling aqueous geochemical systems (Parkhurst and Appelo 2013). It is a modular, reactive-transport geochemical modeling code that is designed to perform a wide range of geochemical calculations, like the calculation of chemical equilibrium, kinetics, ion exchange, mineral dissolution and precipitation, transport processes, etc. Phreeqc uses a database of chemical reactions and thermodynamic data to perform its calculations. The program can be used to model a wide range of geochemical systems, including groundwater, surface water, soils, and sedimentary rocks (Repentigny, Zagury, and Courcelles 2019; Tale et al. 2020).

Phreeqc is particularly well-suited for modeling complex geochemical systems and is widely used by scientists and engineers in a variety of fields, including environmental science, geology, and hydrology. The program is highly customizable and can be used to model a wide range of scenarios, from simple

reactions between a few species to complex multi-component systems with hundreds of species. Phreeqc uses an equilibrium constant method, where mass balance equations are derived from mass action relations. This results in a system of nonlinear equations (Baqer and Chen 2022).

In this work, Phreeqc was utilized to create a model for MICP experiments in a column. This is a common laboratory setup used to study MICP (B. Martinez, DeJong, and Ginn 2014; Phua and Røyne 2018). Phreeqc handles various geochemical calculations using different keyword blocks. A keyword block is a code segment in the input file processed by Phreeqc. To develop a model for conducting MICP in a column, we utilized the following keyword blocks for specific purposes:

- `Solution`: for defining initial and inlet solutions.
- `Rate`: to define the rate of ureolysis and precipitation.
- `Kinetics`: to add the kinetics using rate equations to the solutions.
- `Transport`: to make a column with specific number of cells and initiate flow.
- `Selected_Output`: to collect output data.

The full description of each of the aforementioned keyword blocks is provided in the Phreeqc manual (Parkhurst and Appelo 2013). The input files used for simulations presented in papers are or will become available publicly.

Chapter 4

Summary of Papers

4.1 Paper I

Razbani, M.A and Jettestuen, E and Røyne, A "Direct Pore-Scale Numerical Simulation of Microbially Induced Calcium Carbonate Precipitation". In: *Water Resources Research*. Vol. 58, no. 2 (2023), DOI: 10.1029/2022WR032988.

4.1.1 Summary

In this work, a pore-scale numerical simulator is developed and presented. This simulator is able to study MICP with direct representation of the pore geometry. It includes a native geochemical solver that enhances the speed of numerical calculations comparing to non-native geochemical solvers. The model of MICP in this paper includes ureolysis, precipitation, geometry evolution, and biomass distribution into account. In this paper, we introduce two effectiveness parameters to quantify up-scaling of pore-scale effects. Also, the effect of biomass distribution on up-scaling is studied. Biomass model in our work is a simple one. We consider biomass not part of mass balance in the geometry but a scalar field that is coupled with the geometry. In this paper, we demonstrate the parts of the process in which pore-scale effects manifest at the macro-scale and identify the parts where they are negligible. The effect of biomass distribution was found to be not important. On the other hand, pH evolution was dominated by pore-scale effects. Our findings improve the understanding of the effects of pore-scale phenomena on MICP.

4.1.2 Comparison to other works

We present a numerical simulator for MICP that has some unique features. Unlike other pore-scale simulators for MICP, it has a native geochemical solver that boosts its performance and speed. Using LB enables us to have a realistic representation of the pore-geometry. For example, this approach is more realistic than pore-network models. That's why we call our simulator a direct numerical simulator. Some of our results are similar to what have been reported in the literature previously. For example, the negligence of pore-scale effects for the most part of the MICP was reported before using a pore-network model (Qin, Hassanizadeh, and Ebigbo 2016). The simulator can be used for including more sophisticated ureolysis rates since it gives local values of chemical components.

4.2 Paper II

Razbani, M.A Røyne, A and Jettestuen, E "A Reactive Transport Model for Microbially Induced Calcium Carbonate Precipitation in Phreeqc". *In review at Acta Geotechnica.*

4.2.1 Summary

Unlike the first paper, this work presents the development of a Darcy-scale simulation tool. The objective of this study is to offer an accurate yet user-friendly simulator for biocementation using MICP in column experiments or similar settings. The process was simulated using the Phreeqc geochemical solver, which is an open-source solver widely recognized in the field. We demonstrate how to utilize the inherent capabilities of Phreeqc to model MICP and validate the results by comparing them with experimental data from the literature. The simulator successfully predicts the outcomes of the experiments.

4.2.2 Comparison to other works

Numerous Darcy scale models exist for MICP. However, the model presented in this work possesses unique characteristics. Firstly, it is open-source, allowing for transparency and accessibility. Additionally, it relies on an open-source geochemical solver, further enhancing its flexibility and adaptability. Moreover, it is designed to be user-friendly, enabling ease of use and intuitive operation. Lastly, the model is computationally efficient, resulting in cost-effective simulations.

4.3 Paper III

Razbani, M.A Røyne, A and Jettestuen, E "Numerical Optimization of Biocementation Through Microbially Induced Calcium Carbonate Precipitation". *Prepared for submission.*

4.3.1 Summary

Building upon our approach in the second paper, we address another highly sought-after question regarding the optimization of biocementation. We have improved and expanded the simulator by integrating Phreeqc within a Python code, enabling the execution of multiple simulations with greater flexibility in selecting input parameters. Furthermore, we introduce an objective function to incorporate various efficiency indices. We demonstrate how the simulator and the optimization approach can be utilized to determine the optimal treatment strategy.

4.3.2 Comparison to other works

Due to the complexity in explaining MICP treatments, most models stop by providing a simulation tool or a model. Including excessive details can hinder certain works from optimizing their key input parameters. Our simulator tool, based on a validated model from the second paper, fills this gap. It not only offers a simulation tool but also provides quantitative metrics for comparing different treatment strategies. Similar to the second paper, our tool adopts an open-source approach, offering MICP researchers a free and practical tool to facilitate their work.

Chapter 5

Outlook

In this thesis, we employed both pore-scale and Darcy-scale approaches to study biocementation through MICP. Each approach provided valuable insights into various aspects of the process.

Our investigation suggests that pore-scale models may not yield significant insights into the geochemical evolution of the process unless an advanced ureolysis model is employed. The available ureolysis kinetic formulas, primarily derived from batch experiments, often do not account for pore-scale effects. It is worth noting that MICP is particularly sensitive to the rate of ureolysis. Therefore, changes in the ureolysis rate at the pore-scale could significantly impact the overall MICP modeling. For instance, we demonstrated the significance of pH gradients at the pore-scale, a factor not considered in conventional ureolysis rate equations.

Another interesting aspect that a pore-scale model can explore is the relationship between porosity and permeability. A 3D model, equipped with nucleation criteria, has the potential to shed light on porosity-permeability relationships. Although this specific aspect was not investigated in this work, it presents an interesting avenue for research in the context of mineral-microbe interactions during cementation, possibly through direct numerical simulations at the pore-scale. The simulator proposed in this work can serve as a starting point for such endeavors.

An area that we did not delve into in this work is the mechanical properties of the biocementation process. Pore-scale models have been employed to study these properties in MICP, either at the single pore-scale or indirectly. Our Darcy-scale studies in this work reveal how hydrochemical properties, such as the SR (related to mechanical properties), change over time and space in a column experiment. Combining the dynamics of such parameters with a pore-scale simulator incorporating nucleation criteria could be a valuable tool for predicting and improving the mechanical properties of biocementation.

When developing pore-scale models, it's crucial to consider the evaluation of uncertainties associated with input parameters. These models often demand a detailed characterization of pore structure and material properties, which can be challenging to obtain with high precision. Minor changes or errors in these parameters can potentially have significant effects on the model's output, rendering the models sensitive to uncertainties. If uncertainty exceeds a certain threshold, the model's outputs may become unreliable to the extent that they are no longer useful.

At the Darcy-scale level, we introduced two simulators in this work. The first is a simple script in Phreeqc, while the other is a more sophisticated code in Python, each serving its unique purpose. These tools were developed to facilitate

practical aspects of running biocementation or MICP in a general context.

Our intention is to keep the first script in Phreeqc as it is, providing a straightforward pathway for the hydrochemical modeling of biocementation. However, there is room for further extension and improvement in the second simulator. The optimization conducted in this work was one-dimensional, and higher-dimensional optimization would require different algorithms to optimize a set of input parameters. The code could be expanded to establish correlations between hydrochemistry and mechanical properties, making use of appropriate porosity-permeability relationships. Such enhancements would significantly broaden the method's applicability.

Bibliography

Achal, V. et al. (Feb. 2012). "Bioremediation of Pb-contaminated soil based on microbially induced calcite precipitation". In: *Journal of Microbiology and Biotechnology* vol. 22, no. 2, pp. 244–247. ISSN: 1738-8872. DOI: 10.4014/jmb.1108.08033.

Almajed, A. et al. (Dec. 2019). "Enzyme induced biocementated sand with high strength at low carbonate content". In: *Scientific Reports* vol. 9, no. 1, p. 1135. ISSN: 2045-2322. DOI: 10.1038/s41598-018-38361-1.

Aursjø, O. et al. (Mar. 2017). "An improved lattice Boltzmann method for simulating advective–diffusive processes in fluids". In: *Journal of Computational Physics* vol. 332, pp. 363–375. ISSN: 00219991. DOI: 10.1016/j.jcp.2016.12.014.

Bajželj, B., Allwood, J. M., and Cullen, J. M. (July 2013). "Designing climate change mitigation plans that add up". In: *Environmental Science & Technology* vol. 47, no. 14, pp. 8062–8069. ISSN: 0013-936X. DOI: 10.1021/es400399h.

Baqer, Y. and Chen, X. (2022). "A review on reactive transport model and porosity evolution in the porous media". In: *Environmental Science and Pollution Research* vol. 29, no. 32, pp. 47873–47901. ISSN: 0944-1344. DOI: 10.1007/s11356-022-20466-w.

Barkouki, T. H. et al. (Oct. 2011). "Forward and inverse bio-geochemical modeling of microbially induced calcite precipitation in half-meter column experiments". In: *Transport in Porous Media* vol. 90, no. 1, pp. 23–39. ISSN: 0169-3913, 1573-1634. DOI: 10.1007/s11242-011-9804-z.

Biolith® Tile from Biomason (Apr. 2022). URL: https://biomason.com/biolith.

Carslaw, H. S. and Jaeger, J. C. (2011). *Conduction of heat in solids*. Oxford [Oxfordshire]; New York. ISBN: 0-19-853368-3.

Cui, M.-J. et al. (Oct. 2017). "Influence of cementation level on the strength behaviour of bio-cemented sand". In: *Acta Geotechnica* vol. 12, no. 5, pp. 971–986. ISSN: 1861-1125, 1861-1133. DOI: 10.1007/s11440-017-0574-9.

Cuthbert, M. O., McMillan, L. A., et al. (2013). "A Field and Modeling Study of Fractured Rock Permeability Reduction Using Microbially Induced Calcite Precipitation". In: *Environmental Science & Technology* vol. 47, no. 23, pp. 13637–13643. DOI: 10.1021/es402601g.

Cuthbert, M. O., Riley, M. S., et al. (Apr. 2012). "Controls on the rate of ureolysis and the morphology of carbonate precipitated by S. Pasteurii biofilms and limits due to bacterial encapsulation". In: *Ecological Engineering* vol. 41, pp. 32–40. ISSN: 09258574. DOI: 10.1016/j.ecoleng.2012.01.008.

Dadda, A. et al. (Oct. 2017). "Characterization of microstructural and physical properties changes in biocemented sand using 3D X-ray microtomography".

In: *Acta Geotechnica* vol. 12, no. 5, pp. 955–970. ISSN: 1861-1125, 1861-1133. DOI: 10.1007/s11440-017-0578-5.

Decho, A. W. (Feb. 2010). "Overview of biopolymer-induced mineralization: What goes on in biofilms?" In: *Ecological Engineering*. Special Issue: BioGeoCivil Engineering vol. 36, no. 2, pp. 137–144. ISSN: 0925-8574. DOI: 10.1016/j.ecoleng.2009.01.003.

Dillon, R., Fauci, L., and Gaver, D. (Dec. 1995). "A microscale model of bacterial swimming, chemotaxis and substrate transport". In: *Journal of Theoretical Biology* vol. 177, no. 4, pp. 325–340. ISSN: 0022-5193. DOI: 10.1006/jtbi.1995.0251.

Dong, H. et al. (July 2022). "A critical review of mineral–microbe interaction and co-evolution: mechanisms and applications". In: *National Science Review*, nwac128. ISSN: 2095-5138, 2053-714X. DOI: 10.1093/nsr/nwac128.

Dupraz, S. et al. (July 2009). "Experimental and numerical modeling of bacterially induced pH increase and calcite precipitation in saline aquifers". In: *Chemical Geology* vol. 265, no. 1, pp. 44–53. ISSN: 0009-2541. DOI: 10.1016/j.chemgeo.2009.05.003.

Ebigbo, A. et al. (July 2012). "Darcy-scale modeling of microbially induced carbonate mineral precipitation in sand columns". In: *Water Resources Research* vol. 48, no. 7. ISSN: 00431397. DOI: 10.1029/2011WR011714.

Eltarahony, M., Zaki, S., and Abd-El-Haleem, D. (Dec. 2020). "Aerobic and anaerobic removal of lead and mercury via calcium carbonate precipitation mediated by statistically optimized nitrate reductases". In: *Scientific Reports* vol. 10, no. 1, p. 4029. ISSN: 2045-2322. DOI: 10.1038/s41598-020-60951-1.

Fauriel, S. and Laloui, L. (Nov. 2012). "A bio-chemo-hydro-mechanical model for microbially induced calcite precipitation in soils". In: *Computers and Geotechnics* vol. 46, pp. 104–120. ISSN: 0266352X. DOI: 10.1016/j.compgeo.2012.05.017.

Feng, D. et al. (Apr. 2022). "A comparative study of using two numerical strategies to simulate the biochemical processes in microbially induced calcite precipitation". In: *Journal of Rock Mechanics and Geotechnical Engineering* vol. 14, no. 2, pp. 592–602. ISSN: 1674-7755. DOI: 10.1016/j.jrmge.2021.08.013.

Feng, K., Montoya, B. M., and Evans, T. M. (May 2017). "Discrete element method simulations of bio-cemented sands". In: *Computers and Geotechnics* vol. 85, pp. 139–150. ISSN: 0266-352X. DOI: 10.1016/j.compgeo.2016.12.028.

Ghasemi, P. and Montoya, B. M. (Sept. 2022). "Field implementation of microbially induced calcium carbonate precipitation for surface erosion reduction of a coastal plain sandy slope". In: *Journal of Geotechnical and Geoenvironmental Engineering* vol. 148, no. 9, p. 04022071. ISSN: 1943-5606. DOI: 10.1061/(ASCE)GT.1943-5606.0002836.

Golse, F. (Jan. 2005). "Chapter 3 - The Boltzmann Equation and Its Hydrodynamic Limits". In: *Handbook of Differential Equations: Evolutionary Equations*. Ed. by Dafermos, C. M. and Feireisl, E. Vol. 2. Handbook of Differential Equations Evolutionary Equations, pp. 159–301. DOI: 10.1016/S1874-5717(06)80006-X.

Gomez, M. G., Anderson, C. M., et al. (May 2017). "Large-Scale Comparison of Bioaugmentation and Biostimulation Approaches for Biocementation of Sands". In: *Journal of Geotechnical and Geoenvironmental Engineering* vol. 143, no. 5, p. 04016124. ISSN: 1943-5606. DOI: 10.1061/(ASCE)GT.1943-5606.0001640.

Gomez, M. G., Martinez, B. C., et al. (Aug. 2015). "Field-scale bio-cementation tests to improve sands". In: *Proceedings of the Institution of Civil Engineers - Ground Improvement* vol. 168, no. 3, pp. 206–216. ISSN: 1755-0750. DOI: 10.1680/grim.13.00052.

Hiorth, A., Jettestuen, E., Cathles, L., et al. (Mar. 2013). "Precipitation, dissolution, and ion exchange processes coupled with a lattice Boltzmann advection diffusion solver". In: *Geochimica et Cosmochimica Acta* vol. 104, pp. 99–110. ISSN: 00167037. DOI: 10.1016/j.gca.2012.11.019.

Hiorth, A., Jettestuen, E., Cathles, L. M., et al. (2010). "A fully coupled geochemical model with a pore scale lattice Boltzmann simulator - principles and first results". In: *International Symposium of the Society of Core Analysts*. Halifax, Nova Scotia, Canada.

Hommel, J., Cunningham, A. B., et al. (2013). "Numerical investigation of microbially induced calcite precipitation as a leakage mitigation technology". In: *Energy Procedia* vol. 40, pp. 392–397. ISSN: 18766102. DOI: 10.1016/j.egypro.2013.08.045.

Hommel, J., Lauchnor, E., et al. (May 2015). "A revised model for microbially induced calcite precipitation: Improvements and new insights based on recent experiments". In: *Water Resources Research* vol. 51, no. 5, pp. 3695–3715. ISSN: 00431397. DOI: 10.1002/2014WR016503.

International Energy Agency (2023). *Cement*. URL: https://www.iea.org/reports/cement.

Ivanov, V. and Chu, J. (June 2008). "Applications of microorganisms to geotechnical engineering for bioclogging and biocementation of soil in situ". In: *Reviews in Environmental Science and Bio/Technology* vol. 7, no. 2, pp. 139–153. ISSN: 1569-1705, 1572-9826. DOI: 10.1007/s11157-007-9126-3.

Jeanson, S. et al. (2015). "Bacterial colonies in solid media and foods: A review on their growth and interactions with the micro-environment". In: *Frontiers in Microbiology* vol. 6, p. 1284. ISSN: 1664-302X. DOI: 10.3389/fmicb.2015.01284.

Jettestuen, E. (Dec. 2022). *eje74/BioZement: BADChIMP Simulator*. DOI: 10.5281/ZENODO.7462384.

Landa-Marbán, D. et al. (Mar. 2021). "Practical approaches to study microbially induced calcite precipitation at the field scale". In: *International Journal of Greenhouse Gas Control* vol. 106, p. 103256. ISSN: 1750-5836. DOI: 10.1016/j.ijggc.2021.103256.

Lappin-Scott, H. M. and Bass, C. (Aug. 2001). "Biofilm formation: Attachment, growth, and detachment of microbes from surfaces". In: *American Journal of Infection Control* vol. 29, no. 4, pp. 250–251. ISSN: 0196-6553. DOI: 10.1067/mic.2001.115674.

Lichtner, P. C. (Mar. 1985). "Continuum model for simultaneous chemical reactions and mass transport in hydrothermal systems". In: *Geochimica*

et Cosmochimica Acta vol. 49, no. 3, pp. 779–800. ISSN: 00167037. DOI: 10.1016/0016-7037(85)90172-3.

Lichtner, P. C., Steefel, C. I., and Oelkers, E. H. (2019). *Reactive Transport in Porous Media*. Boston. ISBN: 978-1-5015-0979-7.

Liu, N. et al. (May 2023). "Pore-scale spatiotemporal dynamics of microbial-induced calcium carbonate growth and distribution in porous media". In: *International Journal of Greenhouse Gas Control* vol. 125, p. 103885. ISSN: 1750-5836. DOI: 10.1016/j.ijggc.2023.103885.

Martinez, B. C. et al. (Apr. 2012). "Upscaling microbial induced calcite precipitation in 0.5m columns: experimental and modeling results". In: pp. 4049–4059. DOI: 10.1061/41165(397)414. (Visited on 12/12/2023).

Martinez, B., DeJong, J., and Ginn, T. (May 2014). "Bio-geochemical reactive transport modeling of microbial induced calcite precipitation to predict the treatment of sand in one-dimensional flow". In: *Computers and Geotechnics* vol. 58, pp. 1–13. ISSN: 0266352X. DOI: 10.1016/j.compgeo.2014.01.013.

Mehrabi, R. and Atefi-Monfared, K. (July 2022). "A coupled bio-chemo-hydro-mechanical model for bio-cementation in porous media". In: *Canadian Geotechnical Journal* vol. 59, no. 7, pp. 1266–1280. ISSN: 0008-3674. DOI: 10.1139/cgj-2021-0396.

Miftah, A., Khodadadi Tirkolaei, H., and Bilsel, H. (May 2020). "Bio-precipitation of $CaCO_3$ for soil improvement: A Review". In: *IOP Conference Series: Materials Science and Engineering* vol. 800, p. 012037. ISSN: 1757-899X. DOI: 10.1088/1757-899X/800/1/012037.

Minto, J. M., Lunn, R. J., and El Mountassir, G. (Aug. 2019). "Development of a reactive transport model for field-scale simulation of microbially induced carbonate precipitation". In: *Water Resources Research*, 2019WR025153. ISSN: 0043-1397, 1944-7973. DOI: 10.1029/2019WR025153.

Mujah, D., Cheng, L., and Shahin, M. A. (Apr. 2019). "Microstructural and geomechanical study on biocemented sand for optimization of MICP process". In: *Journal of Materials in Civil Engineering* vol. 31, no. 4, p. 04019025. ISSN: 1943-5533. DOI: 10.1061/(ASCE)MT.1943-5533.0002660.

Mujah, D., Shahin, M. A., and Cheng, L. (July 2017). "State-of-the-art review of biocementation by microbially induced calcite precipitation (MICP) for soil stabilization". In: *Geomicrobiology Journal* vol. 34, no. 6, pp. 524–537. ISSN: 0149-0451, 1521-0529. DOI: 10.1080/01490451.2016.1225866.

Murugan, R. et al. (Aug. 2022). "Importance of carbon to nitrogen ratio in microbial cement production: Insights through experiments and genome-scale metabolic modelling". In: *Biochemical Engineering Journal* vol. 186, p. 108573. ISSN: 1369-703X. DOI: 10.1016/j.bej.2022.108573.

Nassar, M. K. et al. (Jan. 2018). "Large-scale experiments in microbially induced calcite precipitation (MICP): reactive transport model development and prediction". In: *Water Resources Research* vol. 54, no. 1, pp. 480–500. ISSN: 0043-1397, 1944-7973. DOI: 10.1002/2017WR021488.

Nemati, M. (Oct. 2003). "Modification of porous media permeability, using calcium carbonate produced enzymatically in situ". In: *Enzyme and Microbial*

Technology vol. 33, no. 5, pp. 635–642. ISSN: 01410229. DOI: 10.1016/S0141-0229(03)00191-1.

Nishimura, I. and Matsubara, H. (May 2021). "Coupling simulation of microbially induced carbonate precipitation and bacterial growth using reaction–diffusion and homogenisation systems". In: *Acta Geotechnica* vol. 16, no. 5, pp. 1315–1330. ISSN: 1861-1133. DOI: 10.1007/s11440-021-01178-w.

Osinubi, K. J. et al. (Jan. 2020). "Review of the use of microorganisms in geotechnical engineering applications". In: *SN Applied Sciences* vol. 2, no. 2, p. 207. ISSN: 2523-3971. DOI: 10.1007/s42452-020-1974-2.

Park, S.-J., Lee, C.-G., and Kim, S.-B. (Sept. 2008). "Quantification of bacterial attachment-related parameters in porous media". In: *Environmental Engineering Research* vol. 13, no. 3, pp. 141–146. ISSN: 1226-1025. DOI: 10.4491/eer.2008.13.3.141.

Parkhurst, D. L. and Appelo, C. (2013). *Description of input and examples for Phreeqc version 3: a computer program for speciation, batch-reaction, one-dimensional transport, and inverse geochemical calculations*. USGS Numbered Series 6-A43. Reston, VA: U.S. Geological Survey, p. 519. DOI: 10.3133/tm6A43.

Pedersen, J. et al. (Sept. 2014). "Improved lattice Boltzmann models for precipitation and dissolution". In: *Transport in Porous Media* vol. 104, no. 3, pp. 593–605. ISSN: 0169-3913, 1573-1634. DOI: 10.1007/s11242-014-0353-0.

Perri, E. et al. (June 2018). "Carbonate and silicate biomineralization in a hypersaline microbial mat (Mesaieed sabkha, Qatar): Roles of bacteria, extracellular polymeric substances and viruses". In: *Sedimentology* vol. 65, no. 4, pp. 1213–1245. ISSN: 00370746. DOI: 10.1111/sed.12419.

Phua, Y. and Røyne, A. (Apr. 2018). "Bio-cementation through controlled dissolution and recrystallization of calcium carbonate". In: *Construction and Building Materials* vol. 167, pp. 657–668. ISSN: 09500618. DOI: 10.1016/j.conbuildmat.2018.02.059.

Paassen, L. A. van et al. (Dec. 2010). "Quantifying biomediated ground improvement by ureolysis: large-scale biogrout experiment". In: *Journal of Geotechnical and Geoenvironmental Engineering* vol. 136, no. 12, pp. 1721–1728. ISSN: 1090-0241. DOI: 10.1061/(ASCE)GT.1943-5606.0000382.

Qin, C.-Z., Hassanizadeh, S. M., and Ebigbo, A. (Nov. 2016). "Pore-scale network modeling of microbially induced calcium carbonate precipitation: Insight into scale dependence of biogeochemical reaction rates". In: *Water Resources Research* vol. 52, no. 11, pp. 8794–8810. ISSN: 00431397. DOI: 10.1002/2016WR019128.

Razbani, M. A., Jettestuen, E., and Røyne, A. (Jan. 2023). "Direct pore-scale numerical simulation of microbially induced calcium carbonate precipitation". In: *Water Resources Research*. ISSN: 0043-1397, 1944-7973. DOI: 10.1029/2022WR032988.

Repentigny, C. d., Zagury, G. J., and Courcelles, B. (Dec. 2019). "Modeling of the clogging in a MgO column used to treat a Ni- and Co-contaminated water and performance prediction for a centripetal radial column". In: *Chemosphere*

vol. 236, p. 124307. ISSN: 0045-6535. DOI: 10.1016/j.chemosphere.2019.07.038.

Song, C. et al. (Feb. 2022). "Compressive strength of micp-treated silica sand with different particle morphologies and gradings". In: *Geomicrobiology Journal* vol. 39, no. 2, pp. 148–154. ISSN: 0149-0451, 1521-0529. DOI: 10.1080/01490451.2021.2020936.

Tale, F. et al. (2020). "Experimental and simulation study of low salinity brine interactions with carbonate rocks". In: *Journal of Petroleum Science and Engineering* vol. 184, p. 106497. ISSN: 0920-4105. DOI: https://doi.org/10.1016/j.petrol.2019.106497.

Tan, Y. et al. (2017). "Microbially induced CaCO3 precipitation: hydraulic response and micro-scale mechanism in porous media". In: *ScienceAsia* vol. 43, no. 1, p. 1. ISSN: 1513-1874. DOI: 10.2306/scienceasia1513-1874.2017.43.001.

Tang, Y. et al. (Mar. 2019). "Research on simulation analysis method of microbial cemented sand based on discrete element method". In: *Advances in Materials Science and Engineering* vol. 2019, pp. 1–13. ISSN: 1687-8434, 1687-8442. DOI: 10.1155/2019/7173414.

Torkzaban, S. et al. (Apr. 2008). "Transport and fate of bacteria in porous media: Coupled effects of chemical conditions and pore space geometry". In: *Water Resources Research* vol. 44, no. 4, 2007WR006541. ISSN: 0043-1397, 1944-7973. DOI: 10.1029/2007WR006541.

Tufenkji, N. (June 2007). "Modeling microbial transport in porous media: Traditional approaches and recent developments". In: *Advances in Water Resources* vol. 30, no. 6-7, pp. 1455–1469. ISSN: 03091708. DOI: 10.1016/j.advwatres.2006.05.014.

Tveit, S. and Landa-Marbán, D. (Mar. 2022). *Field-scale optimization of injection strategies for leakage mitigation using microbially induced calcite precipitation*. DOI: 10.48550/arXiv.2201.00669.

Van Paassen, L. A. (Mar. 2011). "Bio-Mediated Ground Improvement: From Laboratory Experiment to Pilot Applications". In: *Geo-Frontiers 2011*. Dallas, Texas, United States, pp. 4099–4108. ISBN: 978-0-7844-1165-0. DOI: 10.1061/41165(397)419.

Verhaeghe, F. et al. (Mar. 2006). "Lattice-Boltzmann modeling of dissolution phenomena". In: *Physical Review E* vol. 73, no. 3, p. 036316. ISSN: 1539-3755, 1550-2376. DOI: 10.1103/PhysRevE.73.036316.

Wang, X. and Nackenhorst, U. (June 2020). "A coupled bio-chemo-hydraulic model to predict porosity and permeability reduction during microbially induced calcite precipitation". In: *Advances in Water Resources* vol. 140, p. 103563. ISSN: 0309-1708. DOI: 10.1016/j.advwatres.2020.103563.

Wang, Y. et al. (Sept. 2022). "Use of microfluidic experiments to optimize MICP treatment protocols for effective strength enhancement of MICP-treated sandy soils". In: *Acta Geotechnica* vol. 17, no. 9, pp. 3817–3838. ISSN: 1861-1133. DOI: 10.1007/s11440-022-01478-9.

Weathers, T. S. (Sept. 2011). *Modeling of ureolytic calcite precipitation for the remediation of strontium-90 using a variable velocity streamtube ensemble*. ISBN: 978-1-244-64545-5.

Whiffin, V. S., Paassen, L. A. van, and Harkes, M. P. (Jan. 2007). "Microbial Carbonate Precipitation as a Soil Improvement Technique". In: *Geomicrobiology Journal* vol. 24, no. 5, pp. 417–423. DOI: 10.1080/01490450701436505.

Wijngaarden, W. K. van, Paassen, L. A. van, et al. (Feb. 2016a). "A Reactive transport model for biogrout compared to experimental data". In: *Transport in Porous Media* vol. 111, no. 3, pp. 627–648. ISSN: 0169-3913, 1573-1634. DOI: 10.1007/s11242-015-0615-5.

— (Mar. 2016b). "Simulation of front instabilities in density-driven flow, using a reactive transport model for biogrout combined with a randomly distributed permeability field". In: *Transport in Porous Media* vol. 112, no. 2, pp. 333–359. ISSN: 0169-3913, 1573-1634. DOI: 10.1007/s11242-016-0649-3.

Wijngaarden, W. K. van, Vermolen, F. J., et al. (2010). "Modelling the new soil improvement method biogrout: extension to 3D". In: *Numerical Mathematics and Advanced Applications 2009*. Ed. by Kreiss, G. et al. Berlin, Heidelberg, pp. 893–900. ISBN: 978-3-642-11794-7. DOI: 10.1007/978-3-642-11795-4_96.

— (Mar. 2011). "Modelling biogrout: a new ground improvement method based on microbial-induced carbonate precipitation". In: *Transport in Porous Media* vol. 87, no. 2, pp. 397–420. ISSN: 0169-3913, 1573-1634. DOI: 10.1007/s11242-010-9691-8.

— (June 2013). "A mathematical model for Biogrout: Bacterial placement and soil reinforcement". In: *Computational Geosciences* vol. 17, no. 3, pp. 463–478. ISSN: 1420-0597, 1573-1499. DOI: 10.1007/s10596-012-9316-0.

Wiktor, V. and Jonkers, H. M. (2011). "Quantification of crack-healing in novel bacteria-based self-healing concrete". In: *Cement and Concrete Composites* vol. 33, no. 7, pp. 763–770. DOI: 10.1016/j.cemconcomp.2011.03.012.

Wu, Y. et al. (Dec. 2011). "Geophysical monitoring and reactive transport modeling of ureolytically-driven calcium carbonate precipitation". In: *Geochemical Transactions* vol. 12, no. 1, p. 7. ISSN: 1467-4866. DOI: 10.1186/1467-4866-12-7.

Zhang, J., Su, P., and Li, L. (July 2022). "Bioremediation of stainless steel pickling sludge through microbially induced carbonate precipitation". In: *Chemosphere* vol. 298, p. 134213. ISSN: 0045-6535. DOI: 10.1016/j.chemosphere.2022.134213.

Zhang, K. et al. (May 2023). "Microbial-induced carbonate precipitation (MICP) technology: a review on the fundamentals and engineering applications". In: *Environmental Earth Sciences* vol. 82, no. 9, p. 229. ISSN: 1866-6280, 1866-6299. DOI: 10.1007/s12665-023-10899-y.

Zhang, T. and Klapper, I. (May 2014). "Critical occlusion via biofilm induced calcite precipitation in porous media". In: *New Journal of Physics* vol. 16, no. 5, p. 055009. ISSN: 1367-2630. DOI: 10.1088/1367-2630/16/5/055009.

Zhang, X. et al. (Feb. 2020). "Performance evaluation of a MICP-treated calcareous sandy foundation using shake table tests". In: *Soil Dynamics*

and Earthquake Engineering vol. 129, p. 105959. ISSN: 02677261. DOI: 10.1016/j.soildyn.2019.105959.

Papers

Paper I

Direct Pore-Scale Numerical Simulation of Microbially Induced Calcium Carbonate Precipitation

I

Mohammad Amin Razbani, Espen Jettestuen, Anja Røyne

Published in *Water Resources Research*, January 2023, volume 59, issue 1, pp. n/a - n/a. DOI: 10.1029/2022WR032988.

AGU ADVANCING EARTH AND SPACE SCIENCE

Water Resources Research

RESEARCH ARTICLE
10.1029/2022WR032988

Direct Pore-Scale Numerical Simulation of Microbially Induced Calcium Carbonate Precipitation

Mohammad Amin Razbani[1], Espen Jettestuen[2], and Anja Røyne[1]

[1]Njord Centre, Department of Physics, University of Oslo, Oslo, Norway, [2]Norwegian Research Centre AS (NORCE), Bergen, Norway

Key Points:

- Up-scaling parameters are introduced that show how main processes compete for controlling microbially induced calcium carbonate precipitation
- Biomass distribution does not change the up-scaling parameters in a reaction-diffusion scheme
- It is found that pH local distribution is significant and up-scaled pH is different from Darcy-scale model's predictions

Correspondence to:

A. Røyne,
anja.royne@fys.uio.no

Citation:

Razbani, M. A., Jettestuen, E., & Røyne, A. (2023). Direct pore-scale numerical simulation of microbially induced calcium carbonate precipitation. *Water Resources Research*, *59*, e2022WR032988. https://doi.org/10.1029/2022WR032988

Received 9 JUN 2022
Accepted 24 DEC 2022

Abstract Microbially induced calcium carbonate precipitation (MICP) is a promising method for eco-friendly solutions in geotechincal engineering. MICP involves highly coupled processes in geochemistry and bacterial metabolism that take place in a porous medium. Advancement of these processes drives calcite crystal growth which leads to a decrease in porosity and permeability of the medium. Mathematical models are being developed and used to predict the fate of system at different conditions. Micro-scale and local bio-geochemical evolution and its role on the overall macroscopic fate of MICP needs further investigation. In this work, a pore-scale reactive transport model of MICP for biocementation is developed in a closed system. MICP is simulated in a sample porous geometry in 2D using a native geochemical solver and a lattice Boltzmann solver that handles diffusive transport. We present reactive-transport factors to up-scale pore-scale effects and quantify the efficiency of MICP at different stages of the process. Our results show that pore-scale effects on the average concentration of urea and calcium are not significant after the initial 20% of urea have been consumed. On the other hand, the pH evolution in the system is significantly affected by pore-scale effects. We also explored effects of biomass density and biomass distribution on the reactive transport factors, as well as the effect of the urea to calcium ratio on the resulting crystallization patterns. We found that a higher ratio of rate of ureolysis to rate of precipitation leads to more nucleation sites and more uniform calcite precipitation in the geometry.

1. Introduction

MICP has found many applications in construction materials as an eco-friendly alternative (Røyne et al., 2019; Seifan et al., 2016; Yip et al., 2022). The most commonly used process for MICP is the ureolytic pathway, where alkalophilic bacteria hydrolyze urea in an enzymatic reaction mediated by the enzyme urease. In the majority of MICP studies, the choice of urease producing micro organism is *S. pasteurii* which can produce a large amount of urease. Ureolytic calcium carbonate precipitation occurring in a porous bed of unconsolidated sand can bind the sand grains and form what is called biocement (Whiffin et al., 2007). This method has been investigated extensively and showed promising results in different applications including self-healing systems (Yip et al., 2022), bioremediation (J. Zhang et al., 2022), fracture sealing (Cuthbert et al., 2013), and soil-improvement (Ghasemi & Montoya, 2022). In the first step of biocementation, a calcium source, most commonly $CaCl_2$ mixed with water to form a calcium rich solution (Nassar et al., 2018). In the next step, the calcium rich solution is mixed with urea and urease producing bacteria. Bacteria utilize urea as an energy source and hydrolyze it using an enzyme called urease. As a result, the pH and inorganic carbon content in the solution increases. This makes the solution supersaturated with respect to calcium carbonate, and calcium carbonate crystals precipitate. The set of reactions that describe this process is listed in Table 1.

1.1. Biogeochemical Processes in MICP

It has been shown that the most important parameters for controlling the outcome of a biocementation process are the concentration of calcium in the solution, the concentration of dissolved inorganic carbon, pH, and the density of nucleation sites available for crystallization (Hammes & Verstraete, 2002). The main processes describing biocementation can be classified into three different categories. In the first category, there are hydrodynamics of flow inside the porous media. The second category includes the chemical kinetics of the system, such as the rates of precipitation and urea hydrolysis. Lastly, the microbiological evolution of the system should be described, which can include equations for growth and decay of biomass. Key parts of biocementation will be explained with more details below.

Table 1
Main Chemical Reactions in Biocementation Process[a]

No.	Reaction	logK (25°C)
1	$H_2CO_3 \leftrightarrow HCO_3^- + H^+$	−6.352
2	$HCO_3^- \leftrightarrow CO_3^{2-} + H^+$	−10.329
3	$H_2O \leftrightarrow H^+ + OH^-$	−14.0
4	$CO(NH_2)_2 + 2H_2O \rightarrow H_2CO_3 + 2NH_3$	
5	$NH_3 + H^+ \leftrightarrow NH_4^+$	9.23
6	$Ca^{2+} + CO_3^{2-} \leftrightarrow CaCO_3 \downarrow$	8.48
7	$CaOH^+ \leftrightarrow Ca^{2+} + OH^-$	−1.0 to −1.6
8	$CaHCO_3^+ \leftrightarrow Ca^{2+} + HCO_3^-$	−1.106

[a]Parkhurst and Appelo (2013).

The rate of precipitation is determined mainly by the degree of supersaturation of calcite, and by microscopic surface processes (Teng et al., 2000). In this work, only supersaturation is considered for describing the rate of crystal growth, while nucleation is only allowed on given surface sites, randomly assigned at the initiation of the simulations. The rate of dissolution or precipitation of calcite, as a function of supersaturation, can be described using the following model from Palandari and Kharaka (2004):

$$R_p = (k_1 + k_2 a_H)(1 - \Omega), \tag{1}$$

$$\Omega = \frac{a_{CO_3^{2-}} \cdot a_{Ca^{2+}}}{K}, \tag{2}$$

where R_p is rate of dissolution or precipitation in mol $m^{-2}s^{-1}$, and $k_{1,2}$ are constants equal to 1.55×10^{-6} mol $m^{-2}s^{-1}$ and 0.501 mol $m^{-2}s^{-1}$, respectively, at 25°C. Ω is the saturation ratio, $a_{CO_3^{2-}}$ and $a_{Ca^{2+}}$ are the activities of CO_3^{2-} and Ca^{2+}, respectively, and K is the equilibrium constant.

Experimental studies of biocementation show that there can be three distinct steps in precipitation (W. Zhang et al., 2018). In the first step, amorphous calcium carbonate is formed. This phase is highly hydrated and unstable and is transformed to crystalline forms within seconds (Naka & Carney, 2007), first to sub-micron crystals of vaterite, which is an unstable polymorph of calcium carbonate. In the final step, small seeds of vaterite crystals dissolve and re-precipitate as calcite or aragonite, the more stable polymorphs of calcium carbonate. The model of precipitation that is used in this work refers to the latest step in precipitation where super-micron calcite crystals grow.

In biocementation, the precipitation of calcium carbonate is triggered by ureolysis (Equation 4 in Table 1) which is an enzymatic reaction. The kinetics of this reaction can be described by the Michaelis-Menten model (Lauchnor et al., 2015):

$$R_u = R_m \frac{C_u}{C_u + K_M}, \tag{3}$$

in which R_u is the cell dependent rate of ureolysis in mol $CFU^{-1}h^{-1}$, R_m is the maximum rate of ureolysis, C_u is the concentration of urea, and K_M is the concentration of urea where the rate of reaction is half of the maximum. The unit used for measuring biomass concentration in Equation 3 and elsewhere in this paper is based on CFU which stands for colony forming unit. It counts every bacterium in our model as 1 CFU. K_M and R_m depend on specific enzyme-substrate system conditions, mainly the type and amount of enzyme, pH, ionic strength, and temperature (Chang & Chang, 2000).

1.2. Modeling Biocementation

The porosity and permeability evolution in biocementation is of prime concern from a design standpoint. It will also influence the potential course of mineralization as it influences both advective and diffusive transport of reactants. It dictates the mechanical properties of the final product and its potential applications. An understanding of this evolution requires that the geochemical evolution of the system in the porous media is resolved. Due to the heterogeneity of porous media, both the distribution of nucleation sites and biomass and micro-scale reactive transport in the system may be important. Experimental toolboxes are available that capture the micro-scale bio-geochemical evolution of MICP (Kim et al., 2020; Shu et al., 2022; Weinhardt et al., 2021; Zehner et al., 2021, 2020). Pore-scale modeling can be used to investigate such an evolution. It has been shown that models of reactive transport phenomena at the pore-scale make it possible to explain processes that are not easily modeled at the Darcy (continuum) scale, such as the interplay of porous media architecture with other physical and chemical processes (Molins, 2015; Putnis, 2015).

A generic reactive-transport model starts by coupling equations of transport and chemical kinetics to predict the spatial and temporal evolution of flow and concentration of different components in a system (Lichtner, 1985). Direct numerical simulations (DNSs) of reactive-transport at the pore-scale have been used extensively for

studying geochemistry, flow, mineral dissolution and precipitation, biological activity, and their interconnections in porous media (Steefel et al., 2005). The LB method is suitable for studying dissolution and precipitation in pore-scale (Hiorth et al., 2013). Also, reactive transport LB models have been successfully coupled with individual based models representing dynamics of microbial activity (Graf Von Der Schulenburg et al., 2009; Tian & Wang, 2019). In an individual based model, the bacterial population is modeled by attributing growth parameters to individual bacteria.

So far, most numerical models proposed for studying MICP use the Darcy-scale approach (Ebigbo et al., 2012; Fauriel & Laloui, 2012; Hommel et al., 2015; Landa-Marbán et al., 2021; Minto et al., 2019; Tveit & Marbán, 2022). In this approach, a representative elementary volume which is larger than size of a single pore is defined to introduce volume average quantities, such as volumetric porosity, as continuous functions. Several researchers have pointed out limitations of Darcy-scale modeling of MICP. For example, van Wijngaarden et al. (2016) constructed a 1D model for MICP and concluded that more advanced models are needed to take into account pore-scale processes like placement of bacteria and the geometrical evolution of the sample, because averaging these processes into a continuum model poses significant uncertainties. Barkouki et al. (2011) and Martinez et al. (2014) developed a continuum scale reactive-transport model for MICP. They found that the choice of parameters could not lead to a unique solution, and suggested other spatial and temporal variables, such as the distribution of bacteria, should be included.

Pore-scale modeling of MICP has barely been done. Qin et al. (2016) proposed a pore network method for indirect numerical simulations of MICP at the pore-scale. They represented the architecture of the porous media as a network of spherical pores connected with cylindrical throats, and assumed small variations in quantities inside every pore element. They noted that this assumption probably needs to be justified by direct simulations. T. Zhang and Klapper (2014) developed a pore-scale model for a single pore in MICP. Recently, Nishimura and Matsubara (2021) developed a direct pore-scale model for MICP for a single cell with simplified chemistry. There have been other attempts in pore-scale modeling of not just MICP but enzymatically induced calcium carbonate precipitation (von Wolff et al., 2021). Pore-scale reactive transport models coupled with bacterial activity are well established in the field of bioremediation (Tian & Wang, 2019).

In the present study, we develop a pore-scale model of MICP. The DNS of reactive transport is performed using the LB method coupled with a geochemical solver introduced by Hiorth et al. (2013). Bacterial activities are included using an individual based approach. The model is used to build a bottom-up understanding of MICP. This is achieved by developing functional relationships between ureolysis kinetics, mass transport, and mineral precipitation at the micro-scale.

2. Model Development

The biocementation process is dominated by chemical and biological reactions coupled with transport of solutes and the geometrical evolution of the system. The equation of advection-diffusion, which is a conservation equation, can describe such a system:

$$\frac{\partial C_i}{\partial t} + \nabla \cdot \left(C_i \vec{v}\right) = \nabla \cdot (D_i \nabla C_i) + Q_i, \tag{4}$$

in which C_i is concentration of species i, v is the advection velocity, D_i is the diffusion constant, and Q_i is a source term. The advection is important when solutes are injected into a specimen, such as in column experiments with continuous flow (Barkouki et al., 2011; Ebigbo et al., 2012).

In this paper, we model a closed system. In such a system diffusion is the mechanism of transport and the advective part of the flux term is zero. This is relevant for applications with pulsed injections of the calcium rich solution into the specimen, where there is no flow for most of the time when crystallization is taking place (Zehner et al., 2021). We, therefore, set v to zero in Equation 4. In our model, we include Equation 4 for all of the active species listed in Table 1 together with equations for chemical equilibrium, and kinetics of both ureolysis and precipitation, which will be presented later in this paper. The governing equations become a set of non-linear partial differential equations. To solve this set of equations, a reactive-transport model is developed and solved using the LB method.

2.1. The Lattice Boltzmann Method

The lattice Boltzmann method is a numerical modeling approach based on kinetic theory. The variables used in this method are derived from the velocity distributions in the Boltzmann equation, and the macroscopic variables are found as different moment of these distributions (Krüger et al., 2016). The system's geometry is discretized spatially into square nodes. A distribution function is introduced that gives the density of particles in every node and direction as a function of time. This function formulates the fate of a collision by introducing a collision operator:

$$g_\alpha^i(\mathbf{x}+\mathbf{e}_\alpha\delta t, t+\delta t) - g_\alpha^i(\mathbf{x},t) = \Omega_\alpha^i, \tag{5}$$

where g_α^i is the distribution function, $\mathbf{x}$ is the location of each node, $\mathbf{e}$ is a basis velocity, and Ω_α^i is the collision operator. α and i denote velocity direction and species, respectively. In this work, the LB method is used in a two-dimensional geometry with nine basis velocities, which is a common set up of a lattice (Krüger et al., 2016). The Bhathagar-Gross-Krook operator (Qian et al., 1992) is used as a collision operator. This operator is widely used for advection diffusion problems and predicts the effect of a collision based on the difference between the current distribution and equilibrium distributions. The following equations describe the LB method for modeling the diffusion equation (Equation 4):

$$\Omega_\alpha^i = -\frac{\delta t}{\tau}\left[g_\alpha^i(\mathbf{x},t) - g_\alpha^{i,eq}(\rho)\right] + \Delta\Omega_\alpha^i, \tag{6}$$

$$g_\alpha^{i,eq} = w_\alpha C_i, \tag{7}$$

$$\Delta\Omega_\alpha^i = w_\alpha\left(1+\frac{1}{2\tau}\right)Q_i\delta t, \tag{8}$$

$$C_i = \sum_\alpha g_\alpha^i + \frac{1}{2}Q_i\delta t, \tag{9}$$

where g_α^{eq} is an equilibrium distribution function, τ is the relaxation time, $\Delta\Omega_\alpha^i$ is a lattice source term used to include production and consumption of species in chemical reactions, w_α is the weight constant of the lattice, and δt is the time step. The speed in which the system moves toward equilibrium is adjusted using the relaxation time (τ). Using Chapman-Enskog analysis (Chapman et al., 1990), it has been proved that employing Equation 5 with the aforementioned configuration of the lattice at appropriate scale reproduces the diffusion equation in fluids (Equation 4; Wolf-Gladrow, 1995). In this model, physical parameters are related to the LB parameters as follows:

$$D = \frac{1}{3}\left(\tau-\frac{1}{2}\right)\frac{\delta x^2}{\delta t}, \tag{10}$$

where δx and δt are spatial and temporal resolutions respectively.

At the fluid-mineral interface we use a flux boundary condition. In this context, flux is the diffusive flux (g_i^α in Equation 5). There are different approaches for treating heterogeneous reactions in the LB method. We use a link-based method, where the outgoing flux in a specific direction from a wall node is calculated based on the incoming flux from the neighboring node at the opposite direction, and the rate of reaction on the surface (Hiorth et al., 2013; Verhaeghe et al., 2006).

2.2. Biomass Model

In our model, biomass is modeled as a scalar field on top of the diffusive field. In this approach, biomass is not part of the geometry and does not occupy any space there but interacts with it through ureolysis. This simplification is justified by the fact that biomass nodes account for approximately 1% of total nodes in the bulk. Therefore, the bacteria are not part of the mass balance in the LB part of the model. The biomass field is coupled to the diffusion field to see concentration of chemical components and mineral growth. Biomass is regarded as micro-colonies attached to sand grains. Micro-colonies are contrasted from macro-colonies by their size, where micro-colonies have a threshold radius of 100–200μm (Jeanson et al., 2015). Growth in micro-colonies is similar to planktonic growth, and no pH gradient exists inside the colony. We do not add any viable carbon

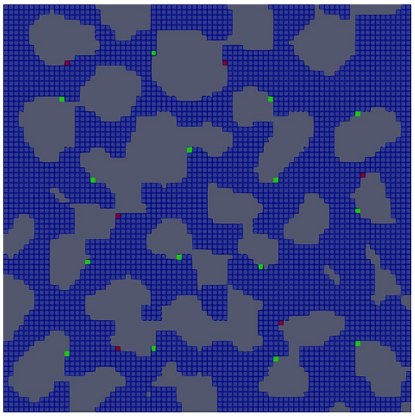

Figure 1. A sample porous geometry (lattice) used in simulating biocementation. Green nodes represent biomass, gray patches are sand grains, and red nodes are nucleation sites.

source or nutrients for the micro-colonies. This is often the case in studies of MICP with a pulsed injection strategy (Lauchnor et al., 2013). Therefore, the micro-colonies do not grow in our simulations, nor do they detach from the surface or break into parts.

Cuthbert et al. (2012) have shown that encapsulation of biomass by calcite crystals limits MICP. In our model, calcite growth in the diffusive field can deactivate biomass wherever they overlap. In this way, the encapsulation and deactivation of bacteria due to calcite growth in MICP can be simulated.

The urease-producing strain used in our model is *S. pasteurii*. The rate of urease production for this strain has been found to be proportional to the biomass concentration (Mobley et al., 1995). Lauchnor et al. (2015) studied MICP using *S. pasteurii* and fit the rate of urea hydrolysis to a Michaelis-Menten relationship for the urea concentration in the range of 1–722 mM. They found the ureolysis rate to be proportional to cell concentration, and reported that NH_4^+, the main product of ureolysis, does not seem to inhibit ureolysis in the range of concentrations relevant for MICP. Considering the findings of Lauchnor et al. (2015) and assuming that only the urea concentration limits ureolysis, we model the kinetics of ureolysis in a biomass node as follows:

$$\frac{dC_u}{dt} = \frac{R_m C_u}{K_M + C_u} C_{sp}, \tag{11}$$

where C_u is the concentration of urea, R_m is the maximum rate constant of ureolysis in a specific biomass concentration and equal to 6.4×10^{-12} mol/CFU/h, K_M is half-saturation constant and equal to 0.305 M, and C_{sp} is the local concentration of *S. pasteurii* bacteria. As we mentioned earlier in this section, in our model the spatial distribution of C_{sp} does not change with time. Although the biomass concentration in a node is constant, biomass nodes can be deactivated due to encapsulation in our model. By doing this, global biomass concentration can change.

2.3. Biomass Density

Experiments have shown that the concentration of *S. pasteurii* in various growth media tends to reach no more than approximately 10^{11} CFU/l (Achal et al., 2009). In the work of Lauchnor et al. (2015), a maximum concentration of $2 \cdot 10^{11}$ CFU/l was reported in their batch experiment with ureolysis. In our model, micro-colonies are placed attached to sand grains. We treat the biomass as unsegregated and unstructured. This means that biomass comprises numerous similar individual agents. The natural disposition of micro-colonies is to fix themselves to a solid surface. Despite this, bacteria can also be found in the bulk in MICP experiments (Lauchnor et al., 2013), but their effect on ureolysis compared to micro-colonies is assumed to be negligible in this work.

S. pasteurii bacteria are rod shaped, approximately 1.3–4.0 μm long and 0.5–1.2 μm in diameter (Bergey & Holt, 1994). We start by a sample porous geometry depicted in Figure 1. Inoculation is done by choosing 15 nodes at the sand surfaces, with the aim of creating the most uniform distribution possible of bacterial micro-colonies. The size of each node is $10^6 \mu m^3$, and we inoculate each node with 400 bacteria. This gives a bulk biomass density of $1.58 \cdot 10^9$CFU/l.

2.4. Lattice Boltzmann Model of MICP

To implement the model introduced in Section 2.2 into the LB solver, we need to evaluate proper source terms from the biomass model and insert them into Equation 6. Because concentration and source terms are coupled, they should be evaluated through solving coupled equations. The following set of equations describe the evolution of urea concentration in LB framework:

$$\frac{dC_u}{dt} = \frac{R_m C_u}{K_M + C_u} C_{sp}, \tag{12}$$

$$\frac{dC_{sp}}{dt} = 0, \tag{13}$$

Table 2
Simulation Set-Up and Properties of the Lattice (Geometry)

Parameter	Value
Initial urea concentration	1.0 M
Initial $CaCl_2$ concentration	1.0 M
Size of the lattice	80 × 80nodes
Length resolution	100μm
Initial porosity	0.57

$$C_u = \rho_u + \frac{1}{2}\frac{dC_u}{dt}, \tag{14}$$

$$\rho_u = \sum_{\alpha} g_{\alpha}. \tag{15}$$

Concentration are defined based on definitions provided in Equations 8 and 9. Solving the equations gives us unknown terms, that is, C_u and dC_u/dt:

$$C_u = -\frac{1}{2}K_u + \frac{1}{2}\rho_u + \frac{1}{4}R_m\rho_s \pm \frac{1}{4}\sqrt{\Delta}, \tag{16}$$

$$\Delta \equiv (2K_M - 2\rho_u - R_m\rho_s)^2 + 16\rho_u K_M. \tag{17}$$

It can be shown that there is only one positive solution for C_u, which is achieved by using a positive sign for $\sqrt{\Delta}$ in Equation 16.

2.5. Nucleation Sites

It has been argued that because bacterial surfaces are negatively charged, they may attract calcium cations and serve as nucleation sites for precipitation (Anbu et al., 2016; Hammes & Verstraete, 2002). This argument has been scrutinized in different studies. Microscale experiments have shown that nano-sized calcite crystals form on the surfaces of bacteria during incipient crystallization (Aloisi et al., 2006; Ghosh et al., 2019). On the other hand, W. Zhang et al. (2018) showed by direct measurements that micrometer-sized crystals are not formed on bacteria's surface but further away from them. Bundeleva et al. (2012) suggested the existence of a cell protection mechanism against calcite incrustation. In this work, biomass encapsulation by calcite is not studied. Therefore, nucleation sites are put at least three nodes away from biomass to avoid biomass encapsulation.

The nucleation regime and the prevalence of nucleation sites during precipitation is important in biocementation. The presence of sand grains introduces heterogeneity into the geometry. Interfaces are formed when solid surfaces meet bulk liquid. These interfaces carry a positive free energy that is called surface energy. The energy barrier for nucleation on these surfaces is lower and therefore nucleation on solid-liquid interfaces is thermodynamically favorable (Kelton & Greer, 2010). No new nucleation site emerges during biocementation in this work.

Different regimes of nucleation and crystal growth lead to different evolution of porosity and permeability and this in turn changes mechanical properties of porous geometry (Stack, 2015), but this is not investigated in this work. In this study, nucleation sites are chosen from fluid nodes on the surfaces of sand grains. They are distributed in a way to have the least discrepancy in the distance among them. Therefore we get an almost even nucleation site distribution. Since nucleation sites are active for precipitation since the beginning of any simulation, the whole process is like a seeded crystallization of calcite. The lowest density of nucleation sites was found by considering the results of Lauchnor et al. (2013), which reported that in their experiments with MICP, the saturation index (SI) would reach a maximum of 3.5. We, therefore, chose the lowest number of nucleation sites in our simulation as an input parameter to yield a saturation index of 3.5 locally at maximum.

2.6. Idealized Models

In order to benchmark the LB simulations, two homogeneous (well-mixed) reaction models of MICP, with the same initial condition as those used for the LB model (Table 2), were constructed in the Phreeqc geochemical solver (Parkhurst & Appelo, 2013). In the first model, system is in equilibrium at each step. Precipitation is modeled by removing calcium carbonate from the bulk until saturation is reached and reactants are added incrementally, and the system is in equilibrium at each step. In the second approach, a kinetic model of MICP was constructed inside Phreeqc. In the kinetic model, Equations 1 and 11 were implemented as rate equations. The geochemical solver in the LB simulator has previously been benchmarked against Phreeqc by Hiorth et al. (2010). They showed that the geochemical solver coupled with the LB model can be compared with experimental data.

2.7. Mass Balance

In our closed system, as calcium carbonate precipitates, calcium and carbonate ions are removed from solution so that the total mass of solution decreases. On the other hand, the precipitated calcium carbonate fills some space

in the pore volume. To track the evolution of the solution volume in a closed system, it is required to calculate the molar volume of aqueous species. The molar volume of ions depends on the ionic strength of the solution and can be calculated using Redlich-type equation (Redlich & Meyer, 1964). Such calculations are not included in the geochemical solver in this work. Periodic boundary conditions are applied at boundaries of the geometry. Therefore, we cannot add and remove fluid from the system without source or sink terms. In this work, the sum of solution volume and volume of precipitated calcite is constant. To check how realistic this assumption is, we calculated the solution volume using Phreeqc which includes proper molar volumes for ions. For the solution described in Table 2, the sum of solution volume and precipitated calcite is not changed til the end when all the initial calcium of 1 M precipitated. Also, the solution volume decreased by 3.7% at the same time.

The change of solution volume changes the concentration of species in the solution. For example, the concentration of inert species should increase a little bit as the pore volume shrinks. In the LB method, this effect is not considered. Physically, It is as if we add some water to the solution and dilute it just enough to compensate for the volume change. Therefore, the concentration of inert species is constant and the effect of change of pore volume on concentrations is ignored. At worst, this will create 3.7% error in the concentrations at the end of each simulation based on the results from Phreeqc. This error is within the uncertainty of the geochemical calculations. These simplifications create a discrepancy in the mass balance over the course of a simulation. The discrepancy in the mass balance is accounted for when simulations are compared with the Phreeqc model. This was done by incorporating the loss of chemical components inside the Phreeqc model based on the data that come from the simulations.

The effect of spatial resolution (δx) was also investigated. The resolution was doubled to see that the LB model can produce consistent results. Comparing concentration of calcium in two different resolutions showed that decreasing the resolution introduces no additional error.

3. Results and Discussions

In the LB model, a 2D geometry represents a biocement specimen. The porous geometry used is depicted in Figure 1. Initial conditions and properties of the system are given in Table 2. The diffusion coefficients for all components in the bulk are considered to be the same and equal to the diffusion coefficient of Ca^{2+} in water. We will see in the next section if this assumption is reasonable. According to Equation 10, the time resolution of our model will be 2.4 s.

3.1. Up-Scaling Pore-Scale Effects

In this section, we up-scale how three main processes in MICP, that is, diffusion, calcite precipitation kinetics and ureolysis kinetics, balance out and control MICP in the whole geometry. To do this, we define two different precipitation factors. The first is the kinetic precipitation factor:

$$\eta_k \equiv \frac{C^i_{Ca} - C^{LB}_{Ca}}{C^i_{Ca} - C^k_{Ca}}, \tag{18}$$

in which i, k, and LB indices refer to the initial condition, the kinetic model, and the LB simulations, respectively. In the idealized system (described in Section 2.6) instead of a porous media, we assume that MICP is happening in a well-mixed bulk. For calculating C^k_{Ca}, we include the kinetics of ureolysis and precipitation and only the effect of diffusion is absent. η_k is a function of reaction progress or amount of calcium precipitated and it should be theoretically between zero and one. The closer η_k becomes to one, the more optimized MICP runs in terms of availability of ureolysis products for precipitation. This means higher rate of precipitation relative to the total amount of calcium precipitated. On the other hand, η_k close to zero means that MICP runs with low rate of precipitation, which is not an optimized condition.

To calculate the η_k, the kinetic model presented in Section 2.6 is used to calculate C^k_{Ca}. In the kinetic model inside Phreeqc, we start by the same amount of reactive surfaces for nucleation that we have inside LB simulation. In Figure 2, the plot of η_k is presented along with concentrations of calcium and urea in the kinetic model and the LB simulations. Figure 2 also shows that the global urea and calcium concentrations in LB simulation, overlap with their counterparts in the kinetic model. Therefore, the effect of diffusion on these parameters in the

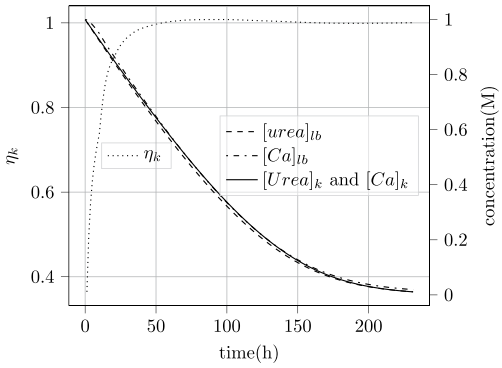

Figure 2. Ureolysis kinetics in an idealized system versus lattice Boltzmann (LB) simulations. Subscripts *lb* and *k* denote LB simulation and the kinetic model respectively. η_k is defined in Equation 18.

pore-scale should be negligible. At the beginning, η_k is close to zero, because right at the beginning there is no precipitation, while ureolysis starts from the first moment. Inspecting reaction rates of ureolysis and precipitation in the Phreeqc model shows that throughout the MICP, reaction rates are equal. Due to slow ureolysis, the same trend is followed in the LB simulations and that is why all concentration profiles almost overlap in Figure 2. We tried two more different initial urea concentration of 0.5 and 2 M. The same trend was observed for rates of precipitation and ureolysis. Therefore we can expect that η_k for different initial concentrations of urea is almost the same.

We call the second type of precipitation factor equilibrium precipitation factor. It quantifies how much calcium is precipitated at each moment in time in the porous media compared to how much would have precipitated if the system was in chemical equilibrium based on the amount of hydrolyzed urea at that moment. The system in chemical equilibrium is the equilibrium model presented in Section 2.6. The equilibrium precipitation factor is defined as follows:

$$\eta_{eq} \equiv \frac{C^i_{Ca} - C^{LB}_{Ca}}{C^i_{Ca} - C^{eq}_{Ca}}, \tag{19}$$

where C^{eq}_{Ca} is the calcium concentration of the equilibrium model. η_{eq} is a measure of how close MICP runs relative to equilibrium. The plot of η_{eq} (Equation 19) is presented in Figure 3. In this figure, one can see that η_{eq} starts off close to zero at the beginning of the MICP and increases sharply to one. As the η_{eq} gets closer to one, the MICP becomes more optimized which means at any urea concentration, a higher amount of calcium is precipitated. As a rule of thumb, in a reaction-diffusion system, as diffusion exerts more control over the whole process (corresponds to high reaction rates), the system distances from equilibrium. On the other hand, if reactions exert more control (corresponding to lower reaction rates), the system gets closer to equilibrium. There are two reaction kinetics in MICP, namely precipitation and ureolysis. Slower ureolysis and faster precipitation gets the system closer to equilibrium. Right at the beginning, the rate of ureolysis is the highest due to higher urea concentration, and the rate of precipitation is the lowest due to lag time it takes for built-up of carbon in the geometry. At the beginning, saturation ratio around nucleation sites is one. As the time goes by, rate of ureolysis decrease and rate of precipitation increases. This means that the system gets closer to equilibrium. From Figure 3, we can say that except the first approximately 20% of the process both in terms of time and urea consumption, the average concentration of calcium in the porous geometry follows the equilibrium model.

More nucleation sites means more reactive surfaces for precipitation, which increases the overall rate of precipitation. Therefore, the ureolysis becomes dominant even sooner in the course of MICP. This means in Figures 2 and 3 the plot of both precipitation factors get closer to one. Since we are already close to equilibrium, higher nucleation densities are not studied. Calcite precipitated at the end of a simulation is shown in Figure 4.

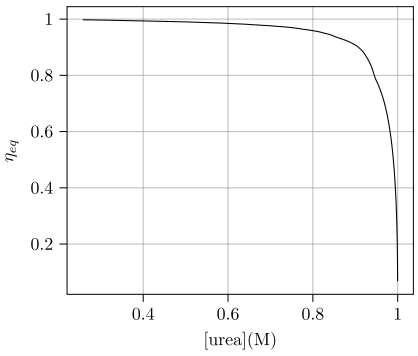

Figure 3. Equilibrium precipitation factor based on Equation 19.

In a non-advective system that we studied, the pore-scale effects are minimized as the reactions get close to equilibrium. In an advective system, pore-scale effects will be pronounced better since fresh reactants are supplied constantly. In such a system, the effect of bacteria transport and attachment would be important. If we lose biomass due to death or encapsulation by calcite, ureolysis rate will get slower and this will shift MICP toward equilibrium even closer. On the other hand, biomass growth in case of supplying nutrients will increase the rate of ureolysis and then we might need to add more nucleation sites. This will need a nucleation criterion to adaptively add nucleation sites in the geometry.

The proposed model and parameters could be used to study other biogeochemical systems involving microbially induced mineral precipitation. Microbially induced carbonates precipitation is used with different microbial

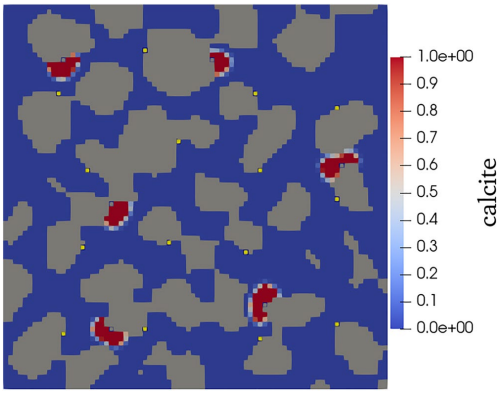

Figure 4. Precipitated calcite at the end of a simulation. Yellow nodes represent biomass, gray patches are sand grains, and gray nodes with edges in the middle of calcite patches are nucleation sites.

groups in addition to ureolytic bacteria for bioremediation of heavy metals from soil through metal carbonate precipitation. Cyanobacteria and algae, nitrate-reducing bacteria, sulfate reducing, ammoniators, and methane oxidants have been used for microbially induced carbonates precipitation (Tamayo-Figueroa et al., 2019).

3.2. Effect of Biomass Distribution and Biomass Density

The effect of biomass distribution on the kinetic and equilibrium precipitation factors was investigated by making different biomass distributions for a single biomass density. Two extra distributions were made by having 30 and 60 biomass nodes in the geometry. These distributions are depicted in Figure 5. Calculating η_{id} and η_{eq} for different biomass distributions showed a negligible deviation of not more than 0.05 between them. It can be concluded that bioamass distribution in the range tested in this work has no effect on η_{id} and η_{eq}. This should be because of the slow rate of ureolysis that gives diffusion enough time to normalize the effect of biomass distribution.

The effect of biomass density on η_{id} and η_{eq} was also tested by decreasing biomass density by two and 10 times of the original biomass density calculated in Section 2.3. Results are shown in Figures 6 and 7. These plots show that decreasing the biomass density shifts η_{id} and η_{eq} toward one, which means that precipitation becomes more efficient. At the same time by decreasing the biomass density, the total time of process increases proportionally. This effect is expected due to the reactive transport nature of MICP described in previous section. By decreasing the biomass density, the system gets closer to the idealized and equilibrium system, introduced in the previous section, because there is more time for the homogenization of the bulk by diffusion.

3.3. Effect of the Initial Conditions

In the last section, we showed that the rate of ureolysis controls the MICP. This rate is the most sensitive to the initial urea concentration according to Equation 11. By increasing the initial urea concentration, the saturation ratio built-up of calcite in the solution is accelerated. There is a maximum saturation ratio before more nucleation sites appear. Saturation ratio cannot increase beyond that maximum because it is thermodynamically unfavorable. Therefore, at higher urea concentrations, more nucleation sites need to be put into the geometry in order to offset the rise of saturation ratio. In this work nucleation sites are always put couple of nodes away from biomass

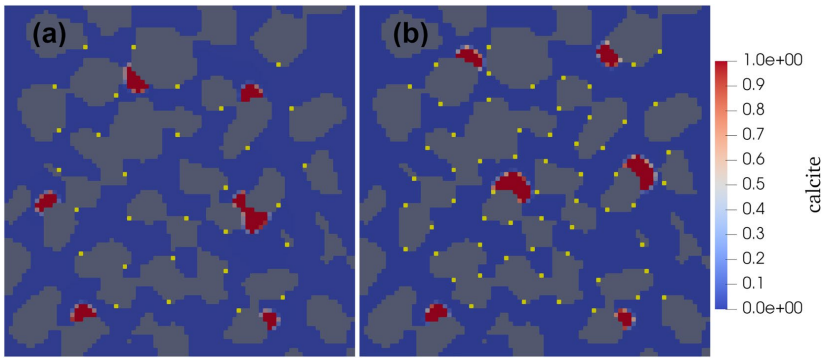

Figure 5. Two different biomass distributions used in simulations of microbially induced calcium carbonate precipitation. Yellow nodes are biomass, red are calcite, gray patches are sand grains and blue shows pore space. The geometry labeled "(a)" has 30 nodes and the one labeled "(b)" has 61 nodes of biomass.

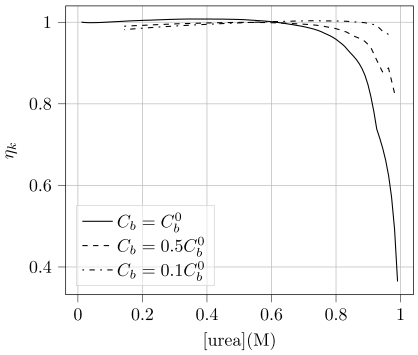

Figure 6. Effect of biomass density (C_b) on η_k (defined in Equation 18), where $C_b^0 = 1.58 \cdot 10^9$ CFU/l.

nodes. Regarding the contrasting findings that were reviewed in Section 2.5, one can assume that a nucleation site happens to be in the same node with a micro-colony in our geometry. In such a case, new rules can be defined in the LB code to handle this situation for deactivating the biomass at appropriate time. By tuning the urea concentration, one can change the number of nucleation sites and this would change the ultimate mechanical properties of MICP. To illustrate this, two extra urea initial conditions are examined in new simulations, at the same conditions mentioned in Table 2 but with urea concentrations of 2 and 0.5 M. For the case of 2 M urea initial concentration, we need to add more nucleation sites to be in the same range of maximum saturation index of 3.5 (like the previous simulations). On the other hand, for the case of 0.5 M initial urea concentration, we need to decrease the number of nucleation sites comparing to the original choice for urea initial concentration of 1 M.

Figure 8 shows when maximum calcium is precipitated at different initial urea concentrations. We can see more nucleation sites at higher urea concentration and vice versa. We do not see any significant change in effectiveness factors with new initial urea concentrations. This is due to the fact that we are in the same range of calcite saturation ratio in all different simulations.

3.4. pH Evolution During MICP

pH is a local parameter in LB simulations. To up-scale pH, we introduce global average pH (pH_{avg}^{LB}) that is calculated from the global arithmetic mean of H^+ concentration. We also introduce $\mathrm{pH}_{\min}^{LB}$ and $\mathrm{pH}_{\max}^{LB}$ in LB simulations as the minimum and maximum pH in the geometry at each step in time. It can be seen from Figure 9 that in the LB simulation pH starts out at a higher value than in the Phreeqc model. The reason is that in LB simulation ureolysis happens instantly from the beginning but precipitation takes time due to transport by diffusion of reactants from biomass sites to nucleation sites. At areas around nucleation sites, precipitation offsets the elevated pH. It is clear from Figure 9 that the effect of pore geometry on pH is significant. In Figure 10, a sample pH distribution in the geometry is presented. It can be seen from the figure that the minimum pH is found around nucleation sites while the maximum pH develops around micro-colonies. The effect of pH on the metabolism of micro-colonies could be important, but it is not investigated in this work. It has been argued that for low Reynolds numbers, biomass creates micro-environments around themselves that leads to a unique precipitation rate (Hammes & Verstraete, 2002). Figure 9 shows that such a local effect can be described well by the LB model.

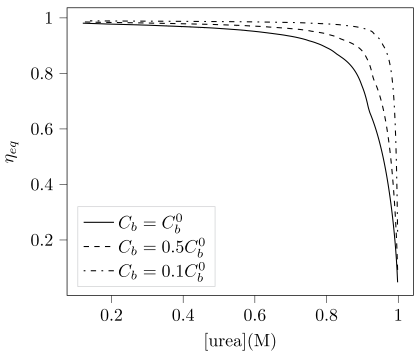

Figure 7. Effect of biomass density (C_b) on η_{eq} (defined in Equation 19), where $C_b^0 = 1.58 \cdot 10^9$ CFU/l.

To find out how sensitive the pH plots are to different choices we made for our case of MICP, different simulations are run. The effect of biomass distribution in terms of number of CFUs in a micro-colony, the number of nucleation sites, and the biomass density as low as one tenth of the original biomass density were tested. Different biomass distribution tested are presented in Figure 5. Results showed that pH development for all simulations are consistent within ±0.1, which is insignificant. Therefore the pH plots presented in Figure 9 should be characteristic of MICP for the case presented in this work and is not sensitive to our choices of biomass density and biomass distribution. This must be because of the fact that rate of ureolysis is not fast enough. Therefore, the biomass density could not change the average pH development. From the other hand, diffusion is fast enough to normalize the effect of biomass distribution. The most important factor here is the initial chemical and geometrical conditions of the system. Changing the initial chemical conditions of the system will change the pH values but not the existence of local pH gradients.

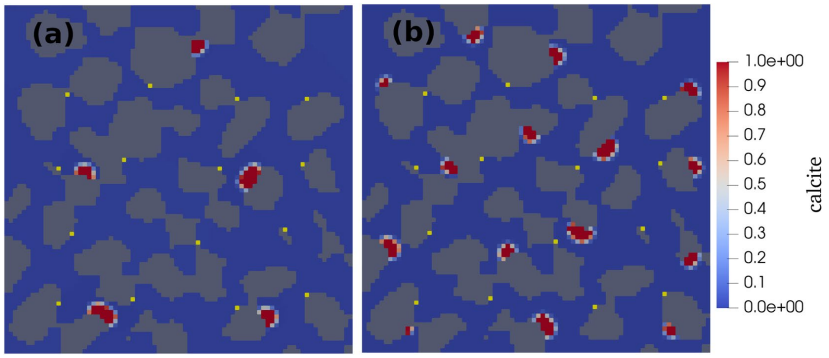

Figure 8. Two different nucleation patterns in simulation of microbially induced calcium carbonate precipitation. Yellow nodes are biomass, red are calcite, gray patches are sand grains and blue shows pore space. The geometry labeled "(a)" starts with 0.5 M urea and the one labeled "(b)" starts with 2 M urea.

4. Conclusion

In this paper, a reactive transport model for biocementation with MICP was developed. A direct numerical simulations of pore-scale MICP was made using the LB method. A simplified model for bacterial ureolysis was implemented that assumes constant ureolysis rate during the course of a simulation.

Two precipitation factors were used to investigate the pore-scale effects. The kinetic precipitation factor showed that except the first 20% of the process, up-scaled kinetics of MICP in our simulations follow the kinetics of an ideal well-mixed system and the process is controlled by the kinetics of ureolysis. Precipitation factors were derived to show how much optimize MICP is running. Equilibrium precipitation factor showed that the system can be considered at equilibrium except for approximately the first 20% of the process.

The biomass distribution was found not to have a significant influence on the precipitation factors. However, the biomass density was found to be important by changing precipitation factors and rate of ureolysis. Significant gradients of local pH were found in the sample, something that is only evident on the pore-scale. Also, the average pH of the system was found to differ from that predicted by the equilibrium model. These observations can be used to improve Darcy-scale models.

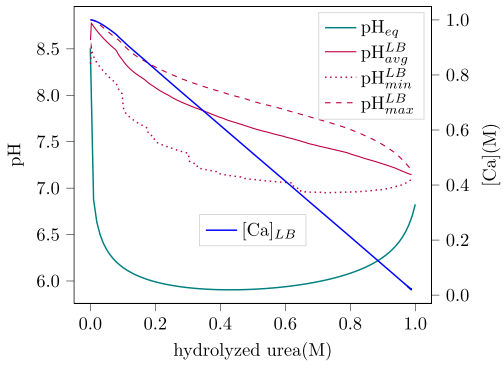

Figure 9. pH evolution of microbially induced calcium carbonate precipitation in lattice Boltzmann simulation in the form of global average (pH^{LB}_{avg}), maximum ($\mathrm{pH}^{LB}_{\mathrm{max}}$), and minimum ($\mathrm{pH}^{LB}_{\mathrm{min}}$) versus reaction progress. pH_{eq} is the corresponding pH from the equilibrium model and $[Ca]_{\mathrm{LB}}$ is the calcium concentration from the LB simulations.

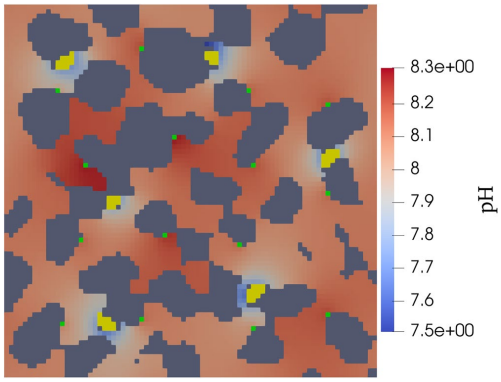

Figure 10. A sample pH distribution during microbially induced calcium carbonate precipitation in lattice Boltzmann simulation. Yellow and green show calcite and biomass, respectively.

While the pore-scale pH evolution in our simulations did not depend on the biomass distribution and biomass density, these factors may be important to include in MICP modeling if the ureolysis kinetics is set to depend on pH. The role of the ratio of urea to calcium initial concentrations on nucleation was explored. With tuning this ratio, one can get different precipitation patterns, considering the properties they expect from the final product. To improve the model presented in this work, a nucleation criterion should be implemented in the model instead of using pre-defined nucleation sites.

Acronyms

MICP	microbially induced calcium carbonate precipitation
LB	lattice Boltzmann
DNS	direct numerical simulation

Data Availability Statement

The code of the LB simulator and a script for Phreeqc simulations can be accessed at Eje74 (2022) and Razbani (2022), respectively.

Acknowledgments
This work was supported by the Research Council of Norway under project 269084/O70.

References

Achal, V., Mukherjee, A., Basu, P. C., & Reddy, M. S. (2009). Strain improvement of *Sporosarcina pasteurii* for enhanced urease and calcite production. *Journal of Industrial Microbiology and Biotechnology*, *36*(7), 981–988. https://doi.org/10.1007/s10295-009-0578-z

Aloisi, G., Gloter, A., Krüger, M., Wallmann, K., Guyot, F., & Zuddas, P. (2006). Nucleation of calcium carbonate on bacterial nanoglobules. *Geology*, *34*(12), 1017–1020. https://doi.org/10.1130/G22986A.1

Anbu, P., Kang, C.-H., Shin, Y.-J., & So, J.-S. (2016). Formations of calcium carbonate minerals by bacteria and its multiple applications. *SpringerPlus*, *5*(1), 250. https://doi.org/10.1186/s40064-016-1869-2

Barkouki, T. H., Martinez, B. C., Mortensen, B. M., Weathers, T. S., De Jong, J. D., Ginn, T. R., et al. (2011). Forward and inverse bio-geochemical modeling of microbially induced calcite precipitation in half-meter column experiments. *Transport in Porous Media*, *90*(1), 23–39. https://doi.org/10.1007/s11242-011-9804-z

Bergey, D., & Holt, J. (1994). *Bergey's manual of determinative bacteriology*. Williams & Wilkins.

Bundeleva, I. A., Shirokova, L. S., Bénézeth, P., Pokrovsky, O. S., Kompantseva, E. I., & Balor, S. (2012). Calcium carbonate precipitation by anoxygenic phototrophic bacteria. *Chemical Geology*, *291*, 116–131. https://doi.org/10.1016/j.chemgeo.2011.10.003

Chang, R., & Chang, R. (2000). *Physical chemistry for the chemical and biological sciences*. University Science Books.

Chapman, S., Cowling, T., Burnett, D., & Cercignani, C. (1990). *The mathematical theory of non-uniform gases: An account of the kinetic theory of viscosity, thermal conduction and diffusion in gases*. Cambridge University Press.

Cuthbert, M. O., McMillan, L. A., Handley-Sidhu, S., Riley, M. S., Tobler, D. J., & Phoenix, V. R. (2013). A field and modeling study of fractured rock permeability reduction using microbially induced calcite precipitation. *Environmental Science & Technology*, *47*(23), 13637–13643. https://doi.org/10.1021/es402601g

Cuthbert, M. O., Riley, M. S., Handley-Sidhu, S., Renshaw, J. C., Tobler, D. J., Phoenix, V. R., & Mackay, R. (2012). Controls on the rate of ureolysis and the morphology of carbonate precipitated by *S. pasteurii* biofilms and limits due to bacterial encapsulation. *Ecological Engineering*, *41*, 32–40. https://doi.org/10.1016/j.ecoleng.2012.01.008

Ebigbo, A., Phillips, A., Gerlach, R., Helmig, R., Cunningham, A. B., Class, H., & Spangler, L. H. (2012). Darcy-scale modeling of microbially induced carbonate mineral precipitation in sand columns: Modeling MICP in porous media. *Water Resources Research*, *48*(7). https://doi.org/10.1029/2011WR011714

Eje74. (2022). eje74/BioZement: BADChIMP Simulator. *Zenodo*. https://doi.org/10.5281/ZENODO.7462384

Fauriel, S., & Laloui, L. (2012). A bio-chemo-hydro-mechanical model for microbially induced calcite precipitation in soils. *Computers and Geotechnics*, *46*, 104–120. https://doi.org/10.1016/j.compgeo.2012.05.017

Ghasemi, P., & Montoya, B. M. (2022). Field implementation of microbially induced calcium carbonate precipitation for surface erosion reduction of a coastal plain sandy slope. *Journal of Geotechnical and Geoenvironmental Engineering*, *148*(9), 04022071. https://doi.org/10.1061/(ASCE)GT.1943-5606.0002836

Ghosh, T., Bhaduri, S., Montemagno, C., & Kumar, A. (2019). *Sporosarcina pasteurii* can form nanoscale calcium carbonate crystals on cell surface. *PLoS One*, *14*(1), e0210339. https://doi.org/10.1371/journal.pone.0210339

Graf Von Der Schulenburg, D. A., Pintelon, T. R. R., Picioreanu, C., Loosdrecht, M. C. M. V., & Johns, M. L. (2009). Three-dimensional simulations of biofilm growth in porous media. *AIChE Journal*, *55*(2), 494–504. https://doi.org/10.1002/aic.11674

Hammes, F., & Verstraete, W. (2002). Key roles of pH and calcium metabolism in microbial carbonate precipitation. *Reviews in Environmental Science and Biotechnology*, *1*(1), 3–7. https://doi.org/10.1023/A:1015135629155

Hiorth, A., Jettestuen, E., Cathles, L. M., Korsnes, R. I., & Madland, M. V. (2010). A fully coupled geochemical model with a pore-scale lattice Boltzmann simulator - principles and first results.

Hiorth, A., Jettestuen, E., Cathles, L. M., & Madland, M. (2013). Precipitation, dissolution, and ion exchange processes coupled with a lattice Boltzmann advection diffusion solver. *Geochimica et Cosmochimica Acta*, *104*, 99–110. https://doi.org/10.1016/j.gca.2012.11.019

Hommel, J., Lauchnor, E., Phillips, A., Gerlach, R., Cunningham, A. B., Helmig, R., et al. (2015). A revised model for microbially induced calcite precipitation: Improvements and new insights based on recent experiments. *Water Resources Research*, *51*(5), 3695–3715. https://doi.org/10.1002/2014WR016503

Jeanson, S., Floury, J., Gagnaire, V., Lortal, S., & Thierry, A. (2015). Bacterial colonies in solid media and foods: A review on their growth and interactions with the micro-environment. *Frontiers in Microbiology*, *6*. https://doi.org/10.3389/fmicb.2015.01284

Kelton, K. F., & Greer, A. L. (2010). Chapter 6—Heterogeneous nucleation. In K. F. Kelton & A. L. Greer (Eds.), *Pergamon Materials Series* (Vol. 15, pp. 165–226). https://doi.org/10.1016/S1470-1804(09)01506-5

Kim, D., Mahabadi, N., Jang, J., & Paassen, L. A. v. (2020). Assessing the kinetics and pore-scale characteristics of biological calcium carbonate precipitation in porous media using a microfluidic chip experiment. *Water Resources Research*, *56*, e2019WR025420. https://doi.org/10.1029/2019WR025420

Krüger, T., Kusumaatmaja, H., Kuzmin, A., Shardt, O., Goncalo, S., & Viggen, E. M. (2016). *The lattice Boltzmann method: Principles and practice*. Springer Berlin Heidelberg.

Landa-Marbán, D., Tveit, S., Kumar, K., & Gasda, S. E. (2021). Practical approaches to study microbially induced calcite precipitation at the field scale. *International Journal of Greenhouse Gas Control*, *106*, 103256. https://doi.org/10.1016/j.ijggc.2021.103256

Lauchnor, E., Schultz, L. N., Bugni, S., Mitchell, A. C., Cunningham, A. B., & Gerlach, R. (2013). Bacterially induced calcium carbonate precipitation and Strontium coprecipitation in a porous media flow system. *Environmental Science & Technology*, *47*(3), 1557–1564. https://doi.org/10.1021/es304240y

Lauchnor, E., Topp, D., Parker, A., & Gerlach, R. (2015). Whole cell kinetics of ureolysis by *Sporosarcina pasteurii*. *Journal of Applied Microbiology*, *118*(6), 1321–1332. https://doi.org/10.1111/jam.12804

Lichtner, P. C. (1985). Continuum model for simultaneous chemical reactions and mass transport in hydrothermal systems. *Geochimica et Cosmochimica Acta*, *49*(3), 779–800. https://doi.org/10.1016/0016-7037(85)90172-3

Martinez, B., De Jong, J., & Ginn, T. (2014). Bio-geochemical reactive transport modeling of microbial induced calcite precipitation to predict the treatment of sand in one-dimensional flow. *Computers and Geotechnics*, *58*, 1–13. https://doi.org/10.1016/j.compgeo.2014.01.013

Minto, J. M., Lunn, R. J., & El Mountassir, G. (2019). Development of a reactive transport model for field-scale simulation of microbially induced carbonate precipitation. *Water Resources Research*, *55*, 7229–7245. https://doi.org/10.1029/2019WR025153

Mobley, H. L., Island, M. D., & Hausinger, R. P. (1995). Molecular biology of microbial ureases. *Microbiological Reviews*, *59*(3), 451–480. https://doi.org/10.1128/mr.59.3.451-480.1995

Molins, S. (2015). Reactive interfaces in direct numerical simulation of pore-scale processes. *Reviews in Mineralogy and Geochemistry*, *80*(1), 461–481. https://doi.org/10.2138/rmg.2015.80.14

Naka, K., & Carney, C. K. (Eds.). (2007). *Biomineralization. 1: Crystallization and self-organization process* (Vol. 270). Springer. (OCLC: 180031509).

Nassar, M. K., Gurung, D., Bastani, M., Ginn, T. R., Shafei, B., Gomez, M. G., et al. (2018). Large-scale experiments in microbially induced calcite precipitation (MICP): Reactive transport model development and prediction. *Water Resources Research*, *54*(1), 480–500. https://doi.org/10.1002/2017WR021488

Nishimura, I., & Matsubara, H. (2021). Coupling simulation of microbially induced carbonate precipitation and bacterial growth using reaction-diffusion and homogenization systems. *Acta Geotechnica*, *16*(5), 1315–1330. https://doi.org/10.1007/s11440-021-01178-w

Palandari, J. L., & Kharaka, Y. K. (2004). A compilation of rate parameters of water-mineral interaction kinetics for application to geochemical modeling (Open-File Report). *U.S. Geological Survey*.

Parkhurst, D. L., & Appelo, C. (2013). *Description of input and examples for Phreeqc version 3: A computer program for speciation, batch-reaction, one-dimensional transport, and inverse geochemical calculations (USGS numbered series No. 6-A43)*. U.S. Geological Survey. https://doi.org/10.3133/tm6A43

Putnis, A. (2015). Transient porosity resulting from fluid-mineral interaction and its consequences. *Reviews in Mineralogy and Geochemistry*, *80*(1), 1–23. https://doi.org/10.2138/rmg.2015.80.01

Qian, Y. H., D'Humières, D., & Lallemand, P. (1992). Lattice BGK models for Navier-Stokes equation. *Europhysics Letters*, *17*(6), 479–484. https://doi.org/10.1209/0295-5075/17/6/001

Qin, C.-Z., Hassanizadeh, S. M., & Ebigbo, A. (2016). Pore-scale network modeling of microbially induced calcium carbonate precipitation: Insight into scale dependence of biogeochemical reaction rates. *Water Resources Research*, *52*(11), 8794–8810. https://doi.org/10.1002/2016WR019128

Razbani, A. (2022). aminraz/Phreeqc: MICP Kinetics. *Zenodo*. https://doi.org/10.5281/ZENODO.7447278

Redlich, O., & Meyer, D. M. (1964). The molal volumes of electrolytes. *Chemical Reviews*, *64*(3), 221–227. https://doi.org/10.1021/cr60229a001

Røyne, A., Phua, Y. J., Balzer Le, S., Eikjeland, I. G., Josefsen, K. D., Markussen, S., et al. (2019). Towards a low CO_2 emission building material employing bacterial metabolism (1/2): The bacterial system and prototype production. *PLoS One*, *14*(4), e0212990. https://doi.org/10.1371/journal.pone.0212990

Seifan, M., Samani, A. K., & Berenjian, A. (2016). Bioconcrete: Next generation of self-healing concrete. *Applied Microbiology and Biotechnology*, *100*(6), 2591–2602. https://doi.org/10.1007/s00253-016-7316-z

Shu, S., Chen, H., & Meng, H. (2022). Modeling microbially induced carbonate precipitation (MICP) in microfluidic porous chips. *Geofluids*, *2022*, e3616473. https://doi.org/10.1155/2022/3616473

Stack, A. G. (2015). Precipitation in pores: A geochemical Frontier. *Reviews in Mineralogy and Geochemistry*, *80*(1), 165–190. https://doi.org/10.2138/rmg.2015.80.05

Steefel, C., Depaolo, D., & Lichtner, P. (2005). Reactive transport modeling: An essential tool and a new research approach for the Earth sciences. *Earth and Planetary Science Letters*, *240*(3–4), 539–558. https://doi.org/10.1016/j.epsl.2005.09.017

Tamayo-Figueroa, D. P., Castillo, E., & Brandão, P. F. B. (2019). Metal and metalloid immobilization by microbiologically induced carbonates precipitation. *World Journal of Microbiology and Biotechnology*, *35*(4), 58. https://doi.org/10.1007/s11274-019-2626-9

Teng, H. H., Dove, P. M., & De Yoreo, J. J. (2000). Kinetics of calcite growth: Surface processes and relationships to macroscopic rate laws. *Geochimica et Cosmochimica Acta*, *64*(13), 2255–2266. https://doi.org/10.1016/S0016-7037(00)00341-0

Tian, Z., & Wang, J. (2019). Lattice Boltzmann simulation of biofilm clogging and chemical oxygen demand removal in porous media. *AIChE Journal*, *65*(9), e16661. https://doi.org/10.1002/aic.16661

Tveit, S., & Marbán, D. L. (2022). Field-scale optimization of injection strategies for leakage mitigation using microbially induced calcite precipitation. https://doi.org/10.13140/RG.2.2.22042.16324

van Wijngaarden, W. K., van Paassen, L. A., Vermolen, F. J., van Meurs, G. A. M., & Vuik, C. (2016). A reactive transport model for biogrout compared to experimental data. *Transport in Porous Media*, *111*(3), 627–648. https://doi.org/10.1007/s11242-015-0615-5

Verhaeghe, F., Arnout, S., Blanpain, B., & Wollants, P. (2006). Lattice-Boltzmann modeling of dissolution phenomena. *Physical Review E*, *73*(3), 036316. https://doi.org/10.1103/PhysRevE.73.036316

von Wolff, L., Weinhardt, F., Class, H., Hommel, J., & Rohde, C. (2021). Investigation of crystal growth in enzymatically induced calcite precipitation by micro-fluidic experimental methods and comparison with mathematical modeling. *Transport in Porous Media*, *137*(2), 327–343. https://doi.org/10.1007/s11242-021-01560-y

Weinhardt, F., Class, H., Vahid Dastjerdi, S., Karadimitriou, N., Lee, D., & Steeb, H. (2021). Experimental methods and imaging for enzymatically induced calcite precipitation in a microfluidic cell. *Water Resources Research*, *57*(3), e2020WR029361. https://doi.org/10.1029/2020WR029361

Whiffin, V. S., van Paassen, L. A., & Harkes, M. P. (2007). Microbial carbonate precipitation as a soil improvement technique. *Geomicrobiology Journal*, *24*(5), 417–423. https://doi.org/10.1080/01490450701436505

Wolf-Gladrow, D. (1995). A lattice Boltzmann equation for diffusion. *Journal of Statistical Physics*, *79*(5–6), 1023–1032. https://doi.org/10.1007/BF02181215

Yip, B., Haniffah, M., Kasiman, E., & Abidin, A. (2022). Research progress on microbial self-healing concrete. *Jurnal Teknologi*, *84*(3), 25–45. https://doi.org/10.11113/jurnalteknologi.v84.17895

Zehner, J., Røyne, A., & Sikorski, P. (2021). A sample cell for the study of enzyme-induced carbonate precipitation at the grain-scale and its implications for biocementation. *Scientific Reports*, *11*(1), 13675. https://doi.org/10.1038/s41598-021-92235-7

Zehner, J., Røyne, A., Wentzel, A., & Sikorski, P. (2020). Microbial-induced calcium carbonate precipitation: An experimental toolbox for in situ and real time investigation of micro-scale pH evolution. *RSC Advances*, *10*(35), 20485–20493. https://doi.org/10.1039/D0RA03897K

Zhang, J., Su, P., & Li, L. (2022). Bioremediation of stainless steel pickling sludge through microbially induced carbonate precipitation. *Chemosphere*, *298*, 134213. https://doi.org/10.1016/j.chemosphere.2022.134213

Zhang, T., & Klapper, I. (2014). Critical occlusion via biofilm induced calcite precipitation in porous media. *New Journal of Physics*, *16*(5), 055009. https://doi.org/10.1088/1367-2630/16/5/055009

Zhang, W., Ju, Y., Zong, Y., Qi, H., & Zhao, K. (2018). In situ real-time study on dynamics of microbially induced calcium carbonate precipitation at a single-cell level. *Environmental Science & Technology*, *52*(16), 9266–9276. https://doi.org/10.1021/acs.est.8b02660

Paper II

A Reactive Transport Model for Microbially Induced Calcium Carbonate Precipitation in Phreeqc.

Mohammad Amin Razbani, Anja Røyne, Espen Jettestuen

Ready for submission,

II

Paper III

Numerical Optimization of Biocementation Through Microbially Induced Calcium Carbonate Precipitation.

Mohammad Amin Razbani, Anja Røyne, Espen Jettestuen

Ready for submission

III